Title: Effect of an algal amendment on the microbial conversion of coal to methane at different sulfate concentrations from the Powder River Basin, USA

Authors: H.J. Smith[1,2*,$], H.D. Schweitzer[1,2*,$,†] E.P. Barnhart[3], W. Orem[4], R. Gerlach[1,5], and M.W. Fields[1,2]

Affiliations: [1]Center for Biofilm Engineering, Montana State University, Bozeman, MT

[2]Department of Microbiology & Cell Biology, Montana State University, Bozeman, MT

[3]U.S. Geological Survey, Wyoming-Montana Water Science Center, Helena, MT

[4]U.S. Geological Survey, Eastern Energy Resources, Reston, VA

[5]Department of Chemical and Biological Engineering, Montana State University, Bozeman, MT

Keywords: methanogenesis; coalbed methane; terrestrial subsurface

[$]H. J. Smith and H.D. Schweitzer contributed equally to this manuscript

[†]Now at Arctic University of Norway, Tromsø, Norway

*Correspondence: H.J. Smith
Center for Biofilm Engineering
366 Barnard Hall
Montana State University
Bozeman, Montana 59717
heidi.smith@montana.edu

H.D. Schweitzer
UiT - The Arctic University of Norway
Hansine Hansens veg 18
9019 Tromsø
Norway
hannah.schweitzer@uit.no

ABSTRACT Biogenic methane is estimated to account for one-fifth of the natural gas worldwide and there is great interest in controlling methane from different sources. Biogenic coalbed methane (CBM) production relies on syntrophic associations between fermentative bacteria and methanogenic archaea to anaerobically degrade recalcitrant coal and produce methanogenic substrates. However, very little is known about how differences in geochemistry, hydrology, and microbial community composition influence subsurface carbon utilization and CBM production. The addition of an amendment consisting of microalgal biomass has previously been shown to increase CBM production while providing the possibility of a closed-

loop fossil system where waste (production water) is used to grow algae to ultimately produce energy (methane). However, the efficiency of enhancing CBM production under different redox conditions remains unresolved. In this study, we focused on the U.S. Geological Survey's Birney test site (Montana, USA) that has nine wells vertically accessing four coal seams with varying geochemistry (low and high sulfate (SO_4^{2-})) and methane production rates. We used organic matter (OM) in the form of algal biomass to discern the effect of this amendment on OM degradation and microbially enhanced CBM production (MeCBM) potential under different geochemical constraints. We tracked changes in community composition, OM composition, organic carbon (OC) concentration, methane production, and nutrients in batch systems over six months. Methane production was detected only in microcosms from low SO_4^{2-} wells (168 to 800 µg methane per gram of coal). The OC consumption varied across time for all wells and the variation was greatest for the low SO_4^{2-} wells. Different groups of syntrophic bacteria were associated with net-carbon consuming microcosms, and specifically *Syntrophorhabdus* was identified with several different statistical methods as a potentially important coal degrader. Results from this study provide insight into potential coal-degraders, the compositional changes in some of the different OM fractions, and trends in carbon consumption related to methane production across coal seams along the vertical SO_4^{2-} gradient.

Introduction

Coal is compositionally dominated by organic carbon (67% to 95%) with an estimated 892 billion tons of carbon currently residing in deep coal reserves (Strapoć et al., 2011). Coalbed methane (CBM) is an unconventional natural gas resource that emits less pollutants than coal-fired power plants during electricity production, and has the potential to utilize existing energy

infrastructure (Kidnay and Parrish, 2006). Biogenic CBM production relies on indigenous, complex microbial communities that contain syntrophic associations between fermentative bacteria and methanogenic archaea (Strapoć et al., 2011). Biogenic CBM production has been recognized to be limited by the recalcitrant nature of coal, resulting in slow conversion of coal into methanogenic substrates (*e.g.*, acetate, an array of low molecular weight compounds, and short chain fatty acids) (Hazen et al., 2012; Strapoć et al., 2011; Wawrik et al., 2012). Previous research indicates that microbe-particle interactions are intrinsic and lead to the decomposition of coal and subsequent methane production (Bouskill et al., 2012; Moore, 2012; Schink, 2005; Strapoć et al., 2011). Evidence for the linkage between coal degradation and the accumulation of methanogenic substrates has been established from laboratory studies (Bouskill et al., 2012; Orem et al., 2010; Strapoć et al., 2011). However, beyond the identification of such organic intermediates in the laboratory, the *in situ* coupling between the biological decomposition of coal and methane production is largely unresolved, especially for coal seams with geochemical constraints that limit methane production. For instance, many coal seams contain SO_4^{2-}, and sulfate-reducing bacteria (SRB) are typically able to out-compete methanogens for substrates (*e.g.*, H_2, acetate, formate) in the presence of SO_4^{2-} because SO_4^{2-} reduction is more energetically favorable than methanogenesis (Muyzer and Stams, 2008; Plugge et al., 2011). Therefore, the presence of different electron acceptors may affect different trophic groups and/or guilds that contribute to the terminal processing of organic carbon during anaerobic mineralization (Muyzer and Stams, 2008) affecting carbon decomposition and potentially microbially enhanced CBM (MeCBM) production.

Current industrial efforts have focused on increasing CBM production through stimulation (*i.e.*, nutrient amendment) and bio-augmentation (Pfeiffer and Ulrich, 2010; Ritter et

al., 2015), and a major goal of these stimulation efforts is to increase microbial numbers and diversity which is often low in coal seams. Some results from stimulation efforts indicate that energy limitation within the subsurface can be overcome via the turnover of biomass and release of nutrients (Hoehler and Jørgensen, 2013) and there is current interest in stimulating MeCBM with algae extract because of the potential to create a longer-term bio-gas system linked to photoautotrophy (Barnhart et al., 2017; Huang et al., 2017). A recent stimulation study demonstrated that the rate of coal-to-methane conversion was increased by ~38% with the addition of algal amendments (Davis et al., 2019) and isotopic results indicated low concentrations of algal amendment increased the coal-to-methane (not the amendment-to-methane) conversion (Davis et al., 2019). While most CBM work has previously been done with low SO_4^{2-} and CBM producing wells (Van Voast, 2003), recent research indicates CBM production can be stimulated in nonproducing and SO_4^{2-} containing coal seams when certain nutrients and methanogenic substrates are supplied (Beckmann et al., 2019; in 't Zandt et al., 2018). While individual inorganic geochemical species have been well described in CBM associated waters (Barnhart et al., 2016; Cheung et al., 2009; Moore, 2012; Ritter et al., 2015; Vinson et al., 2017), the character and composition of organic matter (OM) is largely unexplored. Further work is needed to (i) determine the range of coal conditions that could be amended to enhance CBM production, (ii) understand the effect the amendments have on microbial metabolic capacities under different redox conditions, and (iii) identify shifts in OM composition in different redox environments after amendment addition.

Excitation emission matrix fluorescence spectroscopy (EEMs) is a rapid and nondestructive OM fingerprinting technique that requires small volumes and is capable of differentiation between different source materials (Coble, 1996; Cory and McKnight, 2005).

Within subsurface hydrocarbon environments EEMs has been used to identify anthropogenic organic compounds from hydraulic fracking fluid (Dahm et al., 2012; Lester et al., 2015), to temporally track *in situ* shifts in OM composition (Pope and Herries, 2014), to study biogenic methane stimulation following permanganate treatment (Huang et al., 2013), and to track OM in CBM waste water (Riley et al., 2018). Here, we used EEMs to track the change in soluble OM fractions in microcosms with different coals and SO_4^{2-} levels following amendment addition and varying methane production rates.

Coal associated slurry and water samples were collected from nine wells at the U.S. Geological Survey's (USGS) Birney test site that provide access to four coal seams that have previously been characterized (Fig. 1). The Powder River Basin (PRB) in Wyoming and Montana is one of the largest reserves of low rank, sub-bituminous coal in the world, and contains an estimated 17.4 trillion cubic feet of recoverable CBM (Barnhart et al., 2013; Orem et al., 2010; Strapoć et al., 2011). These coal seams are composed of low-maturity coal and previous studies indicate that the CBM within the PRB is of biogenic origin (Green et al., 2008; Ritter et al., 2015; Strąpoć et al., 2011). The overarching goal of this study was to couple biological and chemical techniques to relate biologically mediated coal degradation with OM composition and methane production through time. We accomplished this by utilizing samples from geochemically diverse PRB coal seams to inoculate microcosms amended with algal biomass to 1) monitor shifts in microbial assemblages to identify potential coal-degrading groups and possible syntrophic interactions, 2) track compositional changes in the water-soluble fluorescent fraction of OM and 3) describe the amendment's effect on the trends in carbon consumption and methane production of CBM microcosms with different redox potentials (*i.e.*, with and without the presence of SO_4^{2-}). Results from this investigation provide insights into the

organisms and environmental conditions responsible for enhanced carbon cycling and methane production.

Materials and Methods

Site Description and Sample Collection

The USGS Birney test site is located in southeastern Montana (45 26 5.975, -106 23 34.760) and consists of nine wells (Fig. 1) accessing four sub-bituminous PRB coal seams in the Paleocene Tongue River Member of the Fort Union Formation: Knobloch (K), Nance (N), Flowers-Goodale (FG), and Terret (T). The heterogeneity of the coal seam hydrogeochemistry and proximate/ultimate analysis of the cores obtained from this site have been described previously (Barnhart et al., 2016) and are summarized in Table S1. Constructed microcosms consisted of coal, formation water, microbial inoculum, and an algal amendment. Coal was collected in July 2011 and 2013. Following collection, cores were placed immediately into sterile bags and temporarily stored on dry ice until they were permanently stored at -80˚C. Formation water was collected from the FG and N coal seams on September 14, 2015 with a Grundfos (Bjerringbro, Denmark) submersible pump for representative low and high SO_4^{2-} water for microcosms. Prior to sample collection, three wellbore volumes were pumped from each well to ensure water from the coal seam and not from the well was collected. Formation water was collected in 6-gallon plastic jugs that had been rinsed three times with the corresponding pumped formation water before being filled. Upon return to the laboratory (Montana State University), water was stored at 4˚C until microcosm set-up. The microbial inoculum was collected using a DMS (Diffusive Microbial Sampler) as previously described (Barnhart et al., 2013; Davis et al.,

2019). On September 14, 2015, a DMS was placed into each of the nine wells included in this study. The DMSs were incubated down-well for 7 months allowing for microbial associations with the coal to occur before DMSs were retrieved. After DMS samples were collected, groundwater was pumped with a Grundfos (Bjerringbro, Denmark) submersible pump on May 9, 2016, from wells K-09, N-11, T-09, and FGP-13. For each well pumped, a combusted and acid washed amber glass bottle was used for filtered (0.22 µm) and unfiltered groundwater and stored on ice for transport to the laboratory for further OM spectral analysis, non-purgeable dissolved organic carbon (NPDOC) concentrations, and anion measurements. Once retrieved, coal slurry from each DMS was aseptically removed and placed into gas-filled (5% CO_2:95% N_2) microcosms, described in more detail below. The remaining DMS coal slurry was placed on dry ice to be transported back to the laboratory for DNA extractions.

Microcosms and Amendments

Coal and formation water were aseptically added to microcosms in the laboratory prior to the addition of inoculum, which was added immediately upon DMS retrieval at the USGS Birney test site. Microcosms were anaerobically prepared in triplicate for both 120-mL serum bottles and 26-mL Balch-type tubes (Davis et al., 2018). Coal core material from the corresponding FG, N, and T coal seams was dried, crushed, and sieved to a size range of 0.85 – 2.0 mm before being added to the microcosm. Coal was added to the microcosms at 1 g/mL of inoculum. Following the addition of coal, microcosms were sealed with butyl rubber stoppers and aluminum crimp seal caps before being degassed with an oxygen-free gas mixture (5% CO_2:95% N_2). Formation water was filtered with a 0.22-µm PES bottle top filter (Thermo Fisher Scientific, Massachusetts, USA) and sparged for 5 hours with the same oxygen-free gas mixture. Filtered formation water (0.22 µm) was added to serum bottles (44 mL) and Balch-type tubes (8 mL),

and all microcosms were amended with an algal suspension. The microalgal amendment (*Chlorella sorokiniana* str. SLA-04) was grown as previously described in photobioreactors (Davis et al., 2019). This algal biomass was previously shown to enhance coal-derived methane production following amendment (Davis et al., 2019). This algal biomass was lyophilized and ground to a fine powder for storage prior to use as an amendment. A stock solution was prepared anoxically using filtered and degassed formation water. All amended treatments received 1 mL of the prepared amendment concentrate to result in a final amendment concentration of 0.1 g/L.

All microcosms were inoculated with DMS slurry from the corresponding well in the field. Serum bottles received 5 mL of inoculum and the Balch-type tubes received 1 mL of inoculum. The initial total liquid volume of all serum bottles was 50 mL and 10 mL for Balch-type tubes, resulting in the same water:coal:amendment:slurry-ratio. To account for potential methane production and abiotic shifts in OM compositions, controls for each well were identically prepared except inoculum was not added and the initial total liquid volume was brought to 50 mL for serum bottles and 10 mL for Balch-type tubes using filtered sterilized formation water. Additional controls excluding algal amendment were run for each treatment condition; methane was not produced in detectable quantities in these controls (data not shown). All microcosms were incubated at room temperature (21±1°C) in the dark for 173 days.

Temporal microcosm sampling and statistical analysis

Methane was analyzed via manual injection of microcosm headspace (1 mL) with a gas chromatograph equipped with a thermal conductivity detector (TCD) interfaced with PeakSimple Chromatography software (Model 8610C, SRI Instruments, Torrance, California, USA). A Supelco HayeSep-D packed stainless-steel column (6 feet × 1/8 in. O.D.) was used with

ultrahigh purity helium carrier gas set at 8 psi of inlet pressure. The oven temperature was set to 40°C and the TCD temperature was set at 150°C. To prevent creating a negative pressure in the tubes, 1 mL of anoxic 5% CO_2:95% N_2 gas was injected to replace the sample volume removed and later accounted for when determining the total amount of methane produced.

Aqueous samples for OM spectral analyses, NPDOC concentrations, anions, cellular abundances, and headspace samples for methane production were collected every 4 weeks on days 5, 33, 61, 89, 117, 145, and 173. In an anaerobic glove bag, slurry (4 mL) from each serum bottle microcosm was removed through the rubber butyl stopper using a sterile 23-G needle. The slurry was filtered through a 0.22-µm cellulose filter into a scintillation vial that had been acid washed and baked at 450°C for 8 hours prior to use. The filtered slurry sample was diluted 1:5 using anoxic Milli-Q (~18 Ω) water prior to spectral characterization in septum-sealed quartz cuvettes in the absence of oxygen. NPDOC samples were diluted 1:4 in Milli-Q water and run on a Formacs TOC/TN Analyzer (Skalar, Netherlands). Low SO_4^{2-} sample anion measurements were performed undiluted while high SO_4^{2-} anion samples were diluted 1:10 with Milli-Q before measurement and analyzed on a Dionex Ion Chromatography System-1100 (Thermo Fisher Scientific, Massachusetts, USA) with 20-minute run times using a 100-µl loop for low SO_4^{2-} and a 20-µl loop for high SO_4^{2-} samples. For all analytical methods, blanks and standard reference curves were obtained following the same protocols. All data were compiled in version 18 Minitab Inc. (State College, Pennsylvania, USA) to determine statistically significant differences across microcosms and temporal data using a general linear model of analysis of variance (ANOVA). The raw data were compiled in relationship to the average of the controls for each time point.

DNA Extractions and Sequencing

DNA was extracted from the slurries using a FastDNA Spin Kit for Soil (MP Biomedical) as previously described (Schweitzer et al., 2019). Before amplification, the DNA was purified using the One Step PCR Clean Up (Zymo Research, California, USA). The bacterial SSU rRNA genes were amplified using a universal prokaryotic 341F-805R primer containing the Illumina adaptor following the MiSeq Sequencing protocol (Takahashi et al., 2014). The archaeal SSU rRNA genes were amplified using 751F-1204R primer (Baker et al., 2003). The PCR products were checked with a 0.8% agarose gel in TAE buffer. The purified PCR amplicons were sequenced with an Illumina MiSeq. PCR clean up, purification, indexing, and DNA concentration normalization using PicoGreen Stain (Quant-IT, Invitrogen) was performed prior to sequencing. The normalized DNA was pooled with a 12.5% PhiX control library. Forward and reverse reads were assembled using QIIME (Caporaso et al., 2010). The sequences were aligned using SILVA and were quality filtered, chimeras were removed, and OTUs and phylotypes were classified with an 80% confidence using the RDP database with Mothur version 1.38.1 (Haas et al., 2011; Quast et al., 2013; Wang et al., 2007). Sequences were deposited in the NCBI SRA database under the BioProject accession number PRJNA737511. Canoco was used to compare the microbial community variations of the initial inoculum and the microcosms using a canonical correspondence analysis (CCA) following protocols set by Leps and Smilauer (2006). The cladograms were created using the Linear Discriminant Analysis Effect Size (LEfSe) analysis following parameters previously described (Segata et al., 2011).

Quantitative PCR

For all DNA extracts that underwent SSU rRNA gene V3/V4 sequencing, quantitative PCR (qPCR) was performed in triplicate on all initial inoculum samples and microcosms after 6-months using bacterial SSU rRNA gene primer 515F-806R with an annealing temperature of 50˚C (Carini et al., 2016) and archaeal SSU rRNA gene primer 109F-912F with an annealing temperature of 60˚C (Imachi et al., 2006). For each reaction there was a 0.4-µM concentration of each primer and 1X high-fidelity Kapa® HiFi HotStart SYBR Fast ReadyMix. All samples were analyzed in technical replicates and 6-month incubations were assayed in biological triplicate with a StepOnePlus Real Time PCR System. Any technical triplicate samples that were greater than 0.5 C_T standard deviation were removed. Fluorescence readings were made after a 72˚C post extension heat step. Standard curves were generated using synthetic DNA g-Blocks® (IDT). Absolute quantification abundance was calculated as the number of gene copies per µl of DNA.

Organic Matter Analysis

Samples for OM spectral characterization were anaerobically collected from aqueous microcosms run in triplicate and filtered through 0.2-µm low-carbon binding filters into septa sealable quartz cuvettes. Following filtration, samples were immediately analyzed at room temperature and if absorbance measurements were > 0.3 (254 nm) samples were diluted with Milli-Q water to minimize inner-filter effects during collection of EEMs (Miller et al., 2010). EEMs were collected with a Fluoromax-4 Spectrofluorometer, equipped with a Xenon lamp light source and a 1-cm pathlength quartz cuvette. Excitation (Ex) wavelengths were scanned from 240-450 nm and emission (Em) wavelengths were recorded between 300 and 550 nm in 2-nm increments, with a 5-nm slit width and 0.25-s data integration time. Post-processing was completed in MATLAB to generate EEMs corrected for inner filter effects, Raman scattering,

and blank water subtraction (Lawaetz and Stedmon, 2009; McKnight et al., 2001). Following EEMs, samples were analyzed for UV-absorbance (190 nm to 1100 nm) with a Genesys 10 Series (Thermo-Scientific) Spectrophotometer with a 1-cm path length cuvette and Milli-Q water as a blank.

For statistical analysis of OM fluorescence, EEMs were decomposed into individual fluorescing components using parallel factor (PARAFAC) (analysis with decomposition routines for excitation emission matrices; drEEM, v. 0.3.0) and the N-way scripts in MATLAB R2016b (Murphy et al., 2013; Stedmon and Bro, 2008). Four individual fluorescing components in the EEMs were identified with PARAFAC, and the identified components were then subjected to chemical characterization and interpretation. A non-negativity constraint was applied to both excitation and emission loadings. The PARAFAC model was validated by split-half analysis with all components of the split model test finding a match with a Tucker correlation coefficient > 0.95 (Murphy et al., 2013). The PARAFAC results are reported with fluorescence maxima (Fmax; Raman Units [R.U.]) for each component over time.

The NPDOC consumption efficiency through time was calculated by standardizing the NPDOC uptake (U) between the final and initial sampling points to create a standard rate of consumption. Uptake was then standardized to the number of gene copies/µl for each sample to calculate the NPDOC consumption efficiency value as previously described (D'Andrilli et al., 2019). The average of all the high and low SO_4^{2-} microcosms was calculated as a group.

$$\left(Initial\ NPDOC\left(\frac{mg}{L}\right) - Final\ NPDOC\left(\frac{mg}{L}\right)\right) = U$$

$$\frac{U}{gene\ copies/\mu l\ of\ DNA} = NPDOC\ conusmption\ efficiency$$

Results

Methane production and carbon utilization

Over the course of incubation, the dissolved fraction of OC was measured using NPDOC. Variations in NPDOC could be divided into three categories which enabled the relationship between carbon utilization and methane production microcosms to be evaluated. Designations consisted of the following: 1) high SO_4^{2-} and non-net carbon consumption (no net loss in NPDOC over time) (K-09 and N-11), 2) low SO_4^{2-} and non-net carbon consumption (FG-11 and FG-09), and 3) low SO_4^{2-} and net carbon consumption (net loss in NPDOC over time) (FGM-13, FGP-13, SS-13, T-11, and T-09) (Fig. 1 and Fig. 2A-B). Initially, NPDOC concentrations were not significantly different ($p=0.35$) across the microcosms inoculated from low SO_4^{2-} coal seam wells (low SO_4^{2-} microcosms). Initial NPDOC concentrations from low SO_4^{2-} microcosms were roughly three times greater than microcosms from high SO_4^{2-} coal seam wells (high SO_4^{2-} microcosms). Final NPDOC concentrations for FG-11 and FG-09 exhibited very little change from the initial NPDOC concentration and were 3.5 times higher compared to the other low SO_4^{2-} microcosms (Table S2). After 6 months of incubation, both the low SO_4^{2-} non-net carbon consumption treatments (FG-11 and FG-09) and the low SO_4^{2-} net-carbon consumption treatments had 9 and 2 times higher NPDOC concentrations compared to the high SO_4^{2-} microcosms. To standardize the amount of NPDOC consumed per cell (number of gene copies), NPDOC consumption efficiency rate was calculated (Table S3). Samples with the highest carbon consumption efficiencies were high SO_4^{2-} wells.

Carbon consumption trends were similar to methane production with net-carbon consuming microcosms producing methane and non-net carbon consumers having low methane production (Fig. 2). Over time, all low SO_4^{2-} microcosms exhibited evidence of methane

production. The greatest methane production corresponded to the low SO_4^{2-} net-carbon consuming microcosms (FGM-13, FGP-13, T-09, SS-13, and T-11) (Fig. 2A). While SS-13 and T-11 generated methane, exponential phase was reached later and the overall methane concentrations were lower compared to FGM-13, FGP-13, and T-09 (Fig. 2A). The low SO_4^{2-} and non-net carbon consuming microcosms had a longer lag-phase and by the end of the 173 days of incubation, rates of methane production were still increasing for these samples (FG-09 and FG-11). Methane production in the low SO_4^{2-} microcosm control (consisting of formation water and coal) had an overall slower rate and lower methane level (Fig. 2A). Methane was not detected above 2.75 µg of methane per gram of coal in any of the high SO_4^{2-} or other control microcosms.

To determine microbial groups that correlated with differences in carbon consumption and methane production, linear discriminant analysis effect size (LEfSe) was used. LEfSe, a phylogenetic biomarker discovery method, was used for class comparison, biological consistency and effect size estimation to determine microorganisms indicative of carbon consumption. At the family level, LEfSe identified Syntrophorhabdaceae, Legionellaceae, Parachlamyidiacea, and Hydrogenedentes to be most prevalent in net-carbon consuming microcosms while *Anaeromyxobacter* was identified as a biomarker for non-net carbon consuming conditions (Fig. S1).

Temporal variation in microbial assemblages

Raw Illumina MiSeq bacterial sequences consisted of 44,187± 54,096 reads per sample and 34,637± 29,895 reads for archaeal sequences. Bacterial quality refined sequence libraries contained on average 10,950 reads, clustered into 1,861 OTUs across all samples. Archaeal

quality refined sequences contained on average 29,035 reads and clustered into 710 OTUs across all samples. On average, all microcosms following incubation increased in lowly abundant (<3%) bacterial OTUs; however, overall diversity decreased across all microcosms, and on average microcosms contained 261±147.8 OTUs for the initial inoculum and decreased to 129.6±54.6 following 6 months of incubation (Fig. 3A, Table S4). Based on Chao richness, the greatest diversity observed in the initial samples was in K-09 with 554 OTUs followed by T-09 with 415 OTUs, and the least diversity was observed in sample N-11 with 107 OTUs (Table S4).

Bacteria. Initial and final bacterial assemblages were predominated by unclassified bacteria and in a majority of microcosms there was an increase in unclassified taxa over time (Fig. S2). To determine which identifiable OTUs were associated with differences in assemblage composition across the different microcosms, unclassified bacteria were removed and not included in relative abundance comparisons. Initial microcosm assemblages were predominated by SRBs from the family Desulfobacteraceae, with an exception to microcosm inoculum SS-13, FGP-13, and T-09 (Fig. 3A). Rather, SS-13, FGP-13, and T-09 inoculum were predominated by sequences indicative of methanotrophs from the family Methylococcaceae and lowly abundant OTUs (<3%) (Fig. 3A).

Initial bacterial assemblages (time zero) clustered together with the exception of N-11 and FGM-13 inocula (Fig. 3B). Following incubation, bacterial assemblages clustered together by well type with the high SO_4^{2-} well microbial assemblages showing high similarity to the initial and control microcosms. There was greater variation observed in microbial assemblage compositions for the low SO_4^{2-} microcosms when compared to initial and control microcosms. The generated bacterial CCA model explained 62.5% of the total variation across all inocula.

There was a 35.8% of variance in the first component indicating that the majority of the variation is attributed to the shift in assemblage compositions for the majority of the low SO_4^{2-} microcosms over the six-month incubation (Fig. 3B). Microcosms FGP-13, FGM-13, N-11, Nance and Knobloch controls observed less variation from the initial inocula. The second component explained 26.7% of the total variance indicating a majority of the variation between the final microcosms (Fig. 3B). After 6 months of incubation, Geobacteraceae and lower abundant OTUs (<3%) dominated bacterial communities in all low SO_4^{2-} microcosms (Fig. 3A-B). There was an increase in lower abundant OTUs (<3%) in high SO_4^{2-} microcosms; however, these microcosms remained predominated by Desulfobacteraceae (Fig. 3A).

Archaea. Microcosms from wells SS-13, FGP-13, and FGM-13 were initially predominated by sequences indicative of Methanobacteriaceae (presumptive hydrogenotrophic) and of the metabolically versatile methanogen, Methanosarcinaceae. Wells FG-11, FG-09, and T-09 were predominated by OTUs closely related to hydrogenotrophic methanogens Methanregulaceae, Methanobacteriaceae, and Methanospirillaceae. Well T-11 was initially predominated by unclassified archaeal sequences (Fig. 3C), whereas high SO_4^{2-} inocula (K-09 and N-11) were predominated by sequences indicative of methylotrophic methanogens from the family Methanomassiliicoccaceae (Fig. 3C). Inoculum for low SO_4^{2-} FGM-13 was predominated by sequences from the family Methanosarcinaceae, and OTUs for T-11 starting inoculum were unclassified (Fig. 3C). Inocula community profiles did not clearly cluster together and were interspersed with final time points closely clustered together based on location. These results indicated that there was little change over time in the sampled archaeal communities and that SO_4^{2-} was a main driver in archaeal assemblage composition (Fig 3D). The generated archaeal

model explained 82% of the total variation over time. The first component explained the majority (68.8%) of the variation between the high and low SO_4^{2-} samples for both initial and final microcosms (Fig. 3D). Differences in archaeal assemblages between the high and low SO_4^{2-} starting inocula and the majority of the incubated high SO_4^{2-} microcosms were explained by the second component (13.2% variance) (Fig. 3D). Incubated low SO_4^{2-} archaeal assemblages were predominated by sequences indicative of Methanoregulaceae (presumptive hydrogenotrophic methanogens). High SO_4^{2-} microcosms shifted to a microbial community dominated by methanogens from the family Methanosarcinaceae, which typically can perform hydrogenotrophic, acetoclastic, and methylotrophic methanogenesis (Fig. 3C). OTUs representative of Methanosaetaceae, typically acetoclastic methanogens, also became much more prevalent over time in all the low SO_4^{2-} microcosms (Fig. 3C).

Bacterial and Archaeal qPCR

Bacterial and archaeal abundances were determined using qPCR. Relatively high variation in bacterial and archaeal gene copy numbers were observed across wells with similar geochemistry due to differences in biomass between treatments (*i.e.* high or low SO_4^{2-}). Conversely, variation across biological replicates on a per well basis was low. The abundance of bacterial SSU rRNA gene sequences for the starting inoculum across all microcosms ranged between 76.2 and 333,471,616 gene copies (Table S5). Maximum bacterial abundances were observed in the initial inoculum from low SO_4^{2-}/net-carbon consuming wells (average 58,919,329 ± 122,723,783 gene copies/µl of DNA) and the lowest gene abundances were observed across all initial low SO_4^{2-}/non-net carbon consuming wells (average 463.33 ± 398.06 gene copies/µl of DNA). Following 6 months of incubation, low SO_4^{2-} non-net carbon

consuming microcosms had an increase in gene copies/µl of DNA compared to a small decrease in bacterial abundance in low SO_4^{2-} net-carbon consuming microcosms. By the end of the incubations the low SO_4^{2-} net-carbon consuming and non-net carbon consuming microcosms were more similar in gene copies/µl for bacteria.

Similar to bacterial results, maximum archaeal abundances were observed in the initial inoculum from low SO_4^{2-}/net-carbon consuming wells (average 106,735 ± 103,944 gene copies/µl of DNA) and minima gene abundances were found across all initial low SO_4^{2-}/non-net carbon consuming wells (average 59.6 ± 43.5 gene copies/µl of DNA). Archaeal abundances in low SO_4^{2-} non-net carbon consuming microcosms increased after incubation, whereas they decreased in low SO_4^{2-} net-carbon consuming microcosms (Table S5).

When gene abundances were compared across high and low SO_4^{2-} microcosms after the 6 month incubations, the high SO_4^{2-} microcosms had a 4.9-fold increase for bacteria while the low SO_4^{2-} microcosms had a 1.7-fold decrease in gene copies/µl of DNA. Archaeal gene copies decreased in copy number by 6 fold in high SO_4^{2-} microcosms and decreased 1.5 fold for low SO_4^{2-} microcosms. When comparing the change from initial to final gene copies/µl of DNA for low SO_4^{2-} non-net carbon consuming there is an increase for both bacteria and archaea, whereas for high SO_4^{2-} there was a smaller 4.9-fold increase (bacteria) and a 6-fold decrease for archaea (Table S5).

OM Analysis

Initial EEMs generated from low and high SO_4^{2-} microcosms showed a high degree of similarity. All EEMs were dominated by peaks fluorescing in the humic-like regions (Fig. 4). Unlike the EEMs from low SO_4^{2-} microcosms, high SO_4^{2-} EEMs also contained fluorescing OM

components at lower excitation and emission wavelengths, and these results indicated microbially derived amino acid-like components (Cory and Kaplan, 2012). There was little variation in OM composition across biological microcosm replicates. Algal amendment reconstituted in sterile deionized water was analyzed in order to discern the contribution of algal amendment to the OM profile of CBM microcosms. EEMs of the algal amendment exhibited fluorescence at low excitation and emission wavelengths. The fluorescence signature of the algal amendment was not apparent in low SO_4^{2-} microcosms, conversely components with similar fluorescence to the algal amendment were apparent in the high SO_4^{2-} microcosms (Fig. S3). Fluorescing OM for all low SO_4^{2-} microcosms changed with a distinct increase of fluorescence at (~ λEm. 425 nm and Ex. 240 and 300 nm) indicative of humic-like material. On the contrary, high SO_4^{2-} microcosms exhibited a notable decrease in amino acid-like fluorescence over time (Em. 300-400 nm and Ex. 240-300 nm), indicating a potential utilization of the algal amendment.

PARAFAC analysis identified four distinct fluorescent components for which the molecular structures are unknown (Fig. 5A-D). Components one and two (C1 and C2) indicated locations of maximum peak intensities typical of what is referred to as humic-like, terrigenous material (Fig. 5A-B) (Coble, 1996). Component three (C3) depicted intermediate characteristics (Logue et al., 2016) in comparison to the other identified components, whereas component four (C4) exhibited fluorescence properties similar to those of the amino acid tryptophan-like microbially derived OM (Cory and Kaplan, 2012). All identified PARAFAC component contributions fluctuated differently over time with minimal fluctuations in abiotic controls. Humic-like C1 showed a substantial increase in intensity over time for all low SO_4^{2-} samples, while there were negligible changes in high SO_4^{2-} samples in comparison to abiotic controls (Fig. 5A). Similar to C1, humic-like C2 had a relative increase in fluorescence over time for low SO_4^{2-}

459 samples; however, this relative increase followed a similar trend in the abiotic controls
460 (indicative of coal components dissolving into solution) but was to a much lesser extent than
461 found in inoculated samples (Fig. 5B). The C3 component increased slightly over time with a
462 greater increase in low SO_4^{2-} samples (Fig. 5C). The trend in C4 intensity shifts were distinct
463 from the temporal trends in the other identified components, and C4 showed a relative decrease
464 over time for high SO_4^{2-} microcosms, while for N-11 the C4 declined to zero (Fig. 5D). A similar
465 utilization trend to N-11 was observed for K-09.
466
467 *Associations between bacterial/archaeal taxa and organic matter (OM) degradation*
468 To determine the relationship between OM composition and microbial assemblages in
469 CBM microcosms, PCA analysis showed relationships between PARAFAC components and
470 bacterial (Fig. 6A) and archaeal groups (Fig. 6B). The established bacterial model explained
471 84.5% (P = 0.002) of the total variation described by the first two axes. The C1 and C2
472 components (humic-like material) trended together and away from C4, tryptophan-like
473 microbially derived OM (Fig. 6A). The first axis explained 47.1% of the variance (P = 0.002)
474 and captured trends between C4 and the other three components (Fig. 6A). Axis II described
475 37.4% of the variation and explained separation between C1 and C2 versus C3 (Fig. 6A). All of
476 the microcosms grouped together with respective triplicate samples. The T-11 microcosms
477 tightly grouped together and correlated with C1 and C2 trends. T-09 and SS-13 microcosms
478 grouped together and correlated with trends in C3 while well FGP-13 grouped together and away
479 from the C3 material. Sequences indicative of Geobacteraceae, Syntrophaceae, Holophagae,
480 Syntrophorhabdaceae, and Flavobacteriaceae were correlated more with C1 and C2 and had a
481 stronger correlation to microbial groups compared to C3 and C4 (Fig. 6A).

The established archaeal model explained 89.2% (P = 0.002) of the total variation across all groups described by the first two axes. The first axis explained 62.5% of the variance (P = 0.002) between separation of identified humic like components (C1 and C2) compared to the intermediate and typtophan-like components (C3 and C4) (Fig. 6B). The archaeal PCA indicated similar trends in the OM components with C1 and C2 trending together and away from C4 as explained by the variation in axis II [26.7% (P=0.002)]. Most of the microcosms grouped with triplicate samples with the exception of FGP-13. Much like the bacterial PCA, the T-11 microcosms correlated with trends in C1 and C2 while T-09 and SS-13 correlated with trends in C3 while FGP-13 did not correlate with trends in C3. Sequences indicative of *Methanolobus* correlated with C4 material while Methanomicrobiales, *Methanosarcina*, and Methanoregulaceae grouped with trends in C3 material (Fig. 6B).

Discussion

Carbon Consumption Linked to Methane Production

In most coal seam microbial studies, the inoculum is retrieved from pumped well water which mainly includes the planktonic communities versus the biofilm communities that are attached to the coal surfaces. In this study, the Diffusive Microbial Sampler (DMS) was used to collect subsurface inoculum. The DMS allows for the attachment of biofilm communities and has been demonstrated to results in increased microbial diversity (Barnhart et al., 2013). By using inoculum directly from the DMSs at the USGS Birney test site, the environmental relevance was maximized (Barnhart et al., 2013), and allowed the microcosms to be ‘K’ selective instead of the traditional ‘R’ selective cultivation strategy, which allowed for organisms that compete most effectively for limiting resources to be selected (Ferrari et al., 2005; Hahn et al., 2004; Watve et al., 2000). Typically, K selective organisms are not the culturable majority but

505 instead consist of the slow-growing heterotrophic and oligotrophic microorganisms that could
506 most likely represent the native populations of the PRB coal seam environments (Watve et al.,
507 2000).

508 After unclassified bacteria were removed, initial bacterial assemblages observed in six of
509 the wells spanning high and low SO_4^{2-} conditions (FG-11, FGM-13, FG-09, T-11, K-09, and N-
510 11) were predominated by sequences indicative of Desulfobacteraceae while the other three were
511 initially predominated by Methylococcaceae. Desulfobacteraceae, a family of well-studied SRB,
512 are capable of survival in a wide range of environments and in the absence of SO_4^{2-} are capable
513 of fermenting organic acids and alcohols (Amend and Teske, 2005; Plugge et al., 2011). In low
514 SO_4^{2-} environments, Desulfobacteraceae might depend on mutualistic relationships with
515 hydrogenotrophic and acetoclastic methanogens during the degradation of complex OM (Plugge
516 et al., 2011; Schink, 2005). Of the six microcosms initially predominated by Desulfobacteraceae,
517 four of the samples were the non-net carbon consuming enrichments (FG-11, FG-09, K-09, and
518 N-11). The shift in predominate organisms from Desulfobacteraceae to Geobacteraeae only
519 occurred in the low SO_4^{2-} microcosms, while the high SO_4^{2-} microcosms maintained dominance
520 in Desulfobacteraceae. The microcosms that shifted to predominately Geobacteraceae produced
521 methane while the Desulfobacteraceae predominate microcosms did not. The community shifts
522 in the microcosms were likely due to both the *in vitro* nature of the experiment as well as the
523 selective pressure of algae amendment and sulfate conditions.

524 New methods, such as MeCBM, are being tested in order to make industrial CBM more
525 economically viable (Davis et al., 2018; Ritter et al., 2015). Many MeCBM methods consist of
526 nutrient additions to stimulate activity of microbial communities, and the more sustainable
527 nutrient, algae, has been reported as a successful stimulant (Barnhart et al., 2013; Davis et al.,

2018; Strapoć et al., 2011; Ulrich and Bower, 2008). Recently, Davis et al. (2018) demonstrated the advantages of optimizing treatments for MeCBM stimulation. Previous research indicates that within unamended high SO_4^{2-} enrichments, SRB would outcompete methanogens which would suppress methane production (Amend and Teske, 2005; Muyzer and Stams, 2008; Plugge et al., 2011; Schink, 2005; Schweitzer et al., 2019), yet under nutrient amended conditions it is possible to increase the hydrocarbon degrading bacterial community and produce methane (Beckmann et al., 2019; Davis et al., 2018, 2019; in 't Zandt et al., 2018). Recent research indicates MeCBM can be stimulated in SO_4^{2-} containing coal seams when certain nutrients and methanogenic substrates are continually supplied (Beckmann et al., 2019; in 't Zandt et al., 2018). Although, both Beckmann et al. (2019) and in 't Zandt et al. (2018) were able to show an increase in methane production of the high SO_4^{2-} Australian coal seam due to acetate amendment, it was still concluded to be an inefficient way to prime MeCBM production (Beckmann et al., 2019). Further work needs to be performed to evaluate the potential for stimulating MeCBM in high SO_4^{2-} environments, but our results also indicate that stimulation of high SO_4^{2-} coal formations using algae is not an efficient way for MeCBM. Yet, the results presented here and from others support the ability to increase the production of coal-associated methane when stimulating a non-producing low SO_4^{2-} coal environment or enhancing that of a producing well. While many of the predominant OTUs in this study have been identified in other coal seams (Surat, Sydney and Bowen Basins of Australia) (Table S1), future work could focus on evaluating the possibility of stimulating the microbial community for MeCBM in different coal seams (Vick et al., 2018).

Within treatments, the extent of methane production tracked with the degree of net NPDOC consumption, with delayed NPDOC consumption correlating to delays in methane

production. Among the low SO_4^{2-} microcosms, there were discrepancies in methane production and NPDOC consumption that were not anticipated. These discrepancies are likely not due to the microbial community composition as the relative abundances in each microcosm indicated similar dominant organisms present in all the low SO_4^{2-} microcosms for both initial and final samplings (Fig 3A & 2C). In addition to possible unknown factors (*e.g.*, presence of toxic metals, variations in coal composition), differences in carbon consumption and methane production are better explained by putative population distributions in the starting inocula respective to the different tested wells, as well as delays based on microbial growth kinetics (Mao et al., 2017; Swinnen et al., 2004). Microcosms could be divided into two categories of low and high SO_4^{2-}, for example, a substantial increase in microbial abundances (SSU rRNA gene qPCR) for low SO_4^{2-} non-net carbon consuming wells compared to small relative increases for the high SO_4^{2-} treatments (Table S5).

While previous research has indicated SRBs will outcompete methanogens under high SO_4^{2-} conditions, it was still anticipated that there would be a high level of microbial activity and hydrocarbon degradation under high SO_4^{2-} and algal amended conditions. Instead, the results showed only a slight increase (4.9-fold increase) in overall gene copies of high SO_4^{2-} bacterial community and the microbial community changed little in terms of the dominant family still being Desulfobacteraceae. As expected, the SO_4^{2-} concentration was a significant selection pressure on the microbial assemblage composition with similar microbial assemblage across all high SO_4^{2-} microcosms (Fig. 3A-D) and on methane production (Fig. 2A). Although, it is surprising that high SO_4^{2-} also correlated with low OM consumption (Fig. 2B) because the Desulfobacteracea family contains many efficient hydrocarbon degrading bacteria. It is possible that there was much more rapid biodegradation and that the majority of carbon was completely

574 degraded into gaseous end products such as CO_2 instead of a solid phase intermediate NPDOC.
575 Although, a greater microbial abundance would be expected in our high SO_4^{2-} microcosms, on
576 average the low SO_4^{2-} microcosms contained 974.5 fold greater gene copy number compared to
577 the high SO_4^{2-} microcosms. This data indicates that the algal amendment was used differently
578 and perhaps not as efficiently as in the presence of the low sulfate in terms of overall biomass
579 loads.
580
581 Organic Matter in Coal Seams
582 With the industrial future of CBM moving towards MeCBM, it is advantageous to
583 understand the relationship between methane production and methanogenic precursors (*i.e.*, OM
584 composition) under stimulated conditions in efforts to maximize methane production. Previous
585 OM related studies within the PRB observed a high rate of OM biodegradation that consists of
586 the removal of long chain *n*-alkanes derived from terrestrial plants, acyclic isoprenoids, alkyl
587 substituted phenanthrenes, trimethyl- and tetramethylnaphthalenes (Formolo et al., 2008).
588 Laboratory bioreactors have demonstrated that *n*-alkanes, *n*-hexadecanoic acid, *n*-octadecanoic
589 acid, β-sitosterol, stigmasterol and phenol organic intermediates have been identified during
590 anaerobic coal biodegradation (Orem et al., 2010). While these studies have identified the
591 occurrence of specific organic intermediates, the broad character of OM over time for coal seams
592 poised at different redox potentials was not established. In the current study, EEMs, a low
593 volume, non-destructive, fingerprinting technique was utilized in combination with microcosms
594 inoculated from nine CBM wells in the PRB. Algal amended microcosms under different SO_4^{2-}
595 conditions were used to understand the relationship between microbial assemblages, dissolved
596 organic matter (DOM) composition, and methane production over time. In general, in situ CBM

formation water is characterized by low DOC concentrations (less than 5 mg/L) (Dahm et al., 2012), and the measured NPDOC from the analyzed microcosms ranged between 1.8 and 11.0 mg/L.

Generated EEMs were similar to previous CBM studies (Dahm et al., 2012; Huang et al., 2013; Riley et al., 2018) and were distinguishable based on the presence or absence of SO_4^{2-}. The primary difference in EEMs between high and low SO_4^{2-} CBM water was the three- to seven-fold increase in fluorescence intensities within low SO_4^{2-} wells and the presence of amino-acid like fluorescence in high SO_4^{2-} waters (Fig. 4). The increase of humic-like organic material in low SO_4^{2-} environments could be the result of coal degradation or altered carbon processing (*i.e.*, methanogenesis that was not observed in high SO_4^{2-} samples). Alternatively, the accumulation of humic-like substances in low SO_4^{2-} conditions could also be a result of substances that are not utilizable under methanogenic conditions compared to sulfate-reducing conditions. The presented results showed four statistically significant regions of fluorescence using PARAFAC modeling (Fig. 4, Fig. 5A-D). There was an increase in C1 and C2 (humic-like substances) and previous research has shown an increase in humic substances from the microbial solubilization of coal (Kulikova et al., 2010; Sekhohola et al., 2013; Valero et al., 2014). Coal is composed of between 50% and 90% humic substances consisting of complex and heterogenous OM (Kulikova et al., 2010; Strapoć et al., 2011; Wawrik et al., 2012), and the bacterial degradation of coal previously demonstrated the generation of N-, C- and H-enriched mature humics (Valero et al., 2014). Similar to previous research demonstrating varying levels of biological coal degradation of coal to humic substances (Sekhohola et al., 2013; Valero et al., 2014), our work demonstrated the biological release of humic-like fractions dependent upon SO_4^{2-} levels. Although, while EEMs is a useful tool because of it is non-destructive nature, sensitivity and low sample volume

requirements, it still has low selectivity for identification of the specific type of carbon compound. It is possible that some of the humic-like substances are lignin-derived low molecular weight aromatics that fluoresce in this same region. Additional work is necessary to best identify the types of OM involved in coal degradation and could incorporate approaches like Gas Chromatography-Mass Spectrometry (GC/MS) analyses to characterize the products of coal biodegradation (Liu et al., 2019).

For high SO_4^{2-} and nonproducing microcosms, the C1, C2 and C3 humic and intermediate substances change very little over time. This could be because the components were not being utilized at all, have a very slow decomposition rate, or could be produced and consumed at the same rate. In previous anaerobic digestion studies (Li et al., 2014), humic components had a similar trend as the high SO_4^{2-} microcosms signifying a consumption of easy to degrade OM such as volatile fatty acids (Cuetos et al., 2010; Tomei et al., 2011). The tryptophan-like C4 substance decreased in high SO_4^{2-} microcosms and were even completely depleted in N-11 microcosms. Tryptophan-like components have previously been identified as being difficult to biodegrade while having the fastest decomposition rate compared to humics and tyrosine in anaerobic environments (Li et al., 2014). The complete loss of tryptophan-like substances and little change in humic-like material in high SO_4^{2-} microcosms may indicate a preferential utilization of the amendment compared to low SO_4^{2-} microcosms that are more likely to be electron acceptor limited (Orem et al., 2007).

Identification of Potentially Important Bacteria Involved in Organic Matter Degradation

The coal seam geochemistry has been relatively stable between 2011-2014 (Table S1). This could be due to low hydraulic conductivity (0.005 m/d) of the coal seams in this region

(Barnhart et al., 2016). Analysis of the microcosms from wells SS-13, FGP-13, and T-09 indicated specific microbial communities play an important role in carbon consumption based on NPDOC and EEMs analysis. Component 1 and 2 identified through EEMs were both indicative of humic-like material that correlated with the sequence distribution of putative microbial groups that have previously been identified as hydrocarbon degrading bacteria (Chen et al., 2016; Zhao et al., 2016). The correlation of hydrocarbon degrading bacteria and the correlation with increasing C1 and C2 humic-like substances (which are likely coal derived) indicates coal biodegradation (Fig. 6A-B). Under methanogenic conditions, Syntrophaceae (*Smithella, Desulfobacca, Syntrophus*) have been described to be capable of degrading hexadecane and contribute to the production of methanogenic precursors such as acetate and hydrogen through the oxidation of alkanes (Cheng et al., 2013; Siddique et al., 2012). *Holophaga* species also have been shown to be important aromatic degrading acetogens (Liesack et al., 1994). Syntrophorhabdaceae contain isolated representatives of known syntrophic acetogens capable of degrading phenol and phthalate in the presence of hydrogenotrophic methanogens and has been previously identified in Sydney, Surat, and Bowen Basin wells (Qiu et al., 2008, 2004; Vick et al., 2018). Flavobacteriaceae have previously been identified in environments with increased levels of carbohydrate-active hydrolases (Cottrell and Kirchman, 2000; Davey et al., 2001; Teeling et al., 2012). All of these organisms likely play a role in increasing carbon availability and providing substrates for methanogenic archaea. Interestingly, there were very few sequences indicative of methanogens or archaea that had a correlation with C1 and C2 humic-like material, but the high-methane producing and net-carbon consuming T-11 microcosms had correlation to shifts in C1 and C2 humic-like material indicative of contrasting taxonomic preferences for DOM processing.

LEfSe associated four bacterial groups including *Candidatus* Hydrogenedentes, Parachlamydiacaea, *Legionella,* and *Syntrophorohabdus* with net-carbon consuming microcosms. Members of the Candidatus Hydrogenedentes Phylum belong to the Fibrobacteres, Chlorobi, Bacteroidetes (FCB) group, and members of this Phylum are putative organic carbon degraders (Nobu et al., 2015). *Legionella* spp. are ubiquitous in aqueous environments and both *Legionella* and Parachlamydiacaea spp. have been described to parasitize and multiply in protozoa indicating that there might be an active eukaryotic community in the coal seams that could be further investigated (Greub and Raoult, 2002; Taylor et al., 2009). *Syntrophorohabdus* belongs to the Syntrophorhabdaceae family which was also identified with the multivariate statistical method presented in this study providing multiple lines of evidence that these are important coal-degrading microorganisms.

Our results also indicated potential methane oxidation as microcosms from wells SS-13, FGP-13, and T-09 were predominated by sequences indicative of Methylococcaceae, a well-studied methanotroph family (Bowman, 2006). Sequences indicative of methanotrophs were observed, particularly in the high methane samples and included Methylococcaceae (*Methylobacter*, *Methylomonas*, *Methylovulum*), and Methylophilaceae (*Methylophilus* and *Methylotenera*) which could explain the decline in methane for these samples (Fig. 2A) (Bowman, 2006; Kalyuzhnaya et al., 2013; Strong et al., 2015). Wells SS-13, FGP-13, and T-09 contained a greater number of OTUs with lowly abundant organisms (<3%). Recent research indicates communal interactions of these methanotrophs with other specific functional guilds, which might allow them to inhabit low oxygen environments (Yu and Chistoserdova, 2017). Additionally, *Methylobacter, Methylomonas* have been identified down-well in both the Sydney and Bowen basins in Australia (Vick et al., 2018). After 6 months of incubation, all the low

SO_4^{2-} microcosms shifted to predominant community members indicative of Geobacteraceae, a well-studied family of organisms associated with the breakdown of complex OM (Chen et al., 2016; Zhao et al., 2016). Previous research using algae amended CBM enrichments have also seen a shift in relative abundance to a Geobacteraceae-predominated community (Davis et al., 2019). Geobacteraceae have also previously been identified in the Ishikari Basin in Japan and Sydney Basin in Australia (Vick et al., 2018).

High SO_4^{2-} wells continued to be predominated by Desulfobacteraceae sequences, and Desulfobacteraceae have been reported to possess great metabolic versatility (*i.e.*, ability to utilize diverse electron sources and fermentative capabilities) (Plugge et al., 2011). In high SO_4^{2-} environments, Desulfobacteraceae could be crucial for the terminal steps for the anaerobic mineralization of OM (Plugge et al., 2011). The variation in carbon consumption across microcosms could be explained by the presence of SO_4^{2-}. In high SO_4^{2-} microcosms there was a near complete utilization of amino acid-like DOM while in low SO_4^{2-} microcosms amino acid-like DOM was temporally transitioning between consumption and production. As previously seen by Stasik et al. (2015) in the presence of SO_4^{2-}, hydrocarbon transformation was inhibited and it is possible that SRB may be competing with hydrocarbon degraders for co-substrates and nutrients (Stasik et al., 2015). SRB also might inhibit hydrocarbon turnover by a buildup of hydrogen sulfide (Reinhard et al., 2005). A buildup of acetate and/or hydrogen during the breakdown of OM has previously been shown to inhibit hydrocarbon degradation (Corseuil et al., 2011; Rakoczy et al., 2011; Schink, 1997).

Shifts in the Archaeal Community Composition

Shifts in the archaeal community were likely due to the precursors produced by the bacterial community. High SO_4^{2-} archaeal assemblages were initially predominated by a presumptive methylotrophic methanogen, Methanomassiliicoccaceae. Methanomassiliicoccaceae have been described to be capable of using a wide range of methylated compounds to produce methane (Borrel et al., 2014). Additionally, methylotrophic methanogens utilize non-competitive substrates and therefore might be able to co-exist with SRB at high levels of SO_4^{2-}. High SO_4^{2-} wells also revealed sequences that were classified as the metabolically versatile methanogen, Methanosarcinaceae. Methanosarcinaceae have been described to use a wide range of substrates including acetate, hydrogen, methanol and CO_2 and have higher potential growth rates than many other methanogens (Jetten et al., 1992; Mara and Horan, 2003).

Unlike with the bacterial analysis, where microcosms had an increase in relative abundance of novel or unclassified organisms, the archaeal analysis indicated a loss in the abundance of novel or unclassified archaea. Both the presence of sequences indicative Methanoregulaceae, a family that contains many hydrogenotrophic methanogens and the presence of Methanosaetaceae that contains previously identified acetoclastic methanogens increased in the low SO_4^{2-} microcosms (Fig. 3C). Methanosaetaceae have been described to have a higher affinity for acetate compared to other acetoclastic methanogens (Jetten et al., 1992; Mara and Horan, 2003). The high SO_4^{2-} microcosms increased in sequences indicative of Methanosarcinaceae but maintained predominant community members consistent with methylotrophic methanogenesis capable of utilizing multiple substrates (Fig. 3C). The shift in these methanogenic communities might be explained by the substrates present in the microcosms. The Geobacteraceae family contains known acetogens that may also indicate an increase in acetate levels. The algae amendment may increase the hydrocarbon degradation of

734 coal to acetate and shift the community to more acetoclastic methanogenesis which has
735 previously been shown as an important metabolism in the Powder River Basin (Davis et al.,
736 2018). When acetate levels are below 1 mM, Methanosaetaceae can become the dominant
737 acetoclastic species with a slower doubling time (3.5-9 days) (Mara and Horan, 2003). As the
738 presumptive acetate is consumed in batch microcosms, the affinity for acetate may favor
739 Methanosaetaceae and hydrogenotrophic methanogenesis (Mara and Horan, 2003).
740 The T-11 microcosms were predominated by sequences indicative of slow-growing
741 hydrogenotrophic methanogens, Methanoregulaceae, Methanobacteriaceae, and the acetoclastic
742 methanogens Methanosaetaceae. These closely related methanogen isolates have previously been
743 shown to be capable of utilizing substrates, hydrogen and acetate, at lower concentrations (Jetten
744 et al., 1992; Mara and Horan, 2003; Yamamoto et al., 2014). Overall, these results indicate that
745 humic-like organic material is an important driver in community composition. In low SO_4^{2-}
746 conditions, acetoclastic methanogens, such as Methanosaetaceae or Methanosarcinaceae, have
747 the ability to consume acetate, reduce the buildup of acetate and therefore reduce the inhibition
748 of hydrocarbon degraders (Jetten et al., 1992; Mara and Horan, 2003). Syntrophic hydrocarbon
749 degraders such as Syntrophaceae (*Smithella*, *Desulfobacca*, *Syntrophus*) and *Syntrophorhabdus*
750 were observed in microcosms with low SO_4^{2-} concentrations and correlated with DOM
751 components C1 and C2 indicative of more humic-like material (Fig. 6A). Previous research has
752 indicated important syntrophic interactions between *Smithella* and Methanosaetaceae where
753 *Smithella* is involved in the anaerobic conversion of alkanes to acetate during oil degradation,
754 whereas Methanosaetaceae will convert acetate to methane (Zengler et al., 1999). In addition,
755 *Syntrophorhabdus aromaticivorans* can degrade phenol, p-cresol, 4-hydroxybenzoate,
756 isophthalate, and benzoate when associated with H_2-scavenging hydrogenotrophic methanogens.

The results presented here highlight the importance of syntrophic interactions in the anaerobic degradation of complex hydrocarbons, such as coal, under amended conditions. To further resolve the factors promoting the biodegradation of coal to methane, future experimentation could incorporate a carbon mass balance and track specific classes of hydrocarbons while simultaneously monitoring the increase in abundance and diversity of microorganisms. In addition, metagenomic and metatranscriptomic investigations of the syntrophic microorganisms identified in this study could help understand the mechanisms used to degrade coal and produce methane.

Conclusions

Results from this study provide insights into potential coal-degraders, the compositional changes in the water-soluble fluorescent fraction of OM, and trends in carbon consumption related to methane production across coal seams along a vertical SO_4^{2-} gradient. The SO_4^{2-} level affected both the prokaryotic community and the OM transformation, with low SO_4^{2-} samples experiencing an increase of humic-like material and high SO_4^{2-} microcosms nearly depleting all detectable protein-like DOM. Although carbon consumption results indicated that two of the low SO_4^{2-} microcosms (FG-11 and FG-09) were non-carbon consuming and different from the other low SO_4^{2-} microcosms, the prokaryotic community and OM results (*i.e.*, the accumulation of humic-like material) are more similar to the five other low SO_4^{2-} carbon consuming environments (T-11, T-09, FGM-13, FGP-13, and SS-13). While early methane results indicate slow and lagging methane production for the low SO_4^{2-} non-carbon consuming microcosms, methane was produced at much higher rates after 90 days compared to the low SO_4^{2-} carbon consuming microcosms which were producing their highest average methane readings at 90

780 days. Conversely, the high SO_4^{2-} non-carbon consuming microcosms never produced any
781 methane throughout the 173-day duration (nor did they exhibit a change in humics).
782 The current interest in using algal amendment as a possible method for MeCBM
783 production centers around the idea of enhancing the microorganisms that promote coal
784 biodegradation to methane precursors. The goal of MeCBM is not just to increase the amount of
785 methane produced but to increase the amount of coal-derived methane. Therefore, it is important
786 that the stimulant being added is increasing the growth of coal-degrading microorganisms in
787 order to increase the amount of available methanogenic substrates. The amount of SO_4^{2-} present
788 in the sample appears to not only have an effect on the type of organisms present but also on the
789 growth of the microbial community which will directly influence the rate of coal biodegradation.
790 The high SO_4^{2-} microcosms had far less gene copies per µl of DNA compared to the low SO_4^{2-}
791 microcosms. While all the microcosms saw an increase in the relative abundance of unclassified
792 bacteria, the high SO_4^{2-} microcosms maintained Desulfobacteraceae as one of the predominant
793 family members.
794 By relating OM fractions to microbial community members, it was possible to identify
795 which microbial populations correlated with the consumption or production specific OM
796 fractions and this assisted in the identification of coal-degrading populations. Specifically,
797 syntrophic Deltaproteobacteria belonging to the family *Syntrophorhabdaceae* were identified as
798 important coal degraders. *Syntrophaceae* were also identified and are known alkane degraders in
799 subsurface environments containing oil, and *Syntrophorhabdaceae* have been shown to degrade
800 a wide variety of recalcitrant compounds in association with methanogens. However, this is the
801 first time these groups of microorganisms have been associated with coal degradation. Future
802 efforts could focus of cultivation and meta-omic analyses of *Syntrophaceae* and

803 *Syntrophorhabdaceae* to better understand the strategies these microorganisms might use in
804 association with methanogens to enable the dynamic turnover of recalcitrant carbon in the
805 terrestrial subsurface.
806

Acknowledgements

The authors would like to acknowledge the U.S. Geological Survey's Energy Resources Program which provided access to the field site where the samples were collected.

Disclaimer: All data generated or analyzed during this study are included in the main text or supplementary information of this publication. Any use of trade, firm, or product names is for descriptive purposes only and does not imply endorsement by the U.S. Government. We would also like to acknowledge George Platt who contributed towards field collection and sample processing. This research was supported by the National Science Foundation through Grants EAR-1322795 and 1736255 (BuG ReMeDEE) as well as through the U.S. Geological Survey.

Contributions

H.D.S., H.S., and E.P.B wrote the paper. H.D.S., H.S., E.P.B., M.W.F, and W.O. contributed in experimental design. H.D.S., H.S., E.P.B., and R.G. collected samples from the field. H.D.S., H.S., and E.P.B. performed experiments. H.D.S. and H.S. performed analysis. E.P.B., R.G., M.W.F and W.O. critically reviewed the manuscript. M.W.F supervised research.

Competing Interests

The authors declare that there are no competing interests.

Figure Legends

Figure 1. Representation of the Birney test site (modified from Barnhart et al., 2016) which consists of nine wells that access four major PRB coal seams (Knobloch (K), Nance (N), Flowers-Goodale (FG), and Terret (T)). Wells are color coded based on sulfate levels with high

sulfate wells (>20 mM) in blue and low sulfate wells (<0.4 mM) in orange. Wells are additionally labeled according to whether there was an overall net carbon consumption or no net carbon consumption.

Figure 2. (A) Average amount of methane produced (μg) over 6 months for each corresponding microcosm replicate with GC measurements made every 28 days. All measurements were collected in triplicate and vertical lines represent the standard deviation for each time point and sample. (B) Amount of NPDOC for each microcosm treatment divided by control treatments (microcosms without inoculum) over a 6 month incubation (time 0 to 6) with measurements made every 28 days. The horizontal solid black line at 1.0 represents no difference between treatment and control; an increase of $NPDOC_{after}/NPDOC_{before}$ indicates net-production of NPDOC, a decrease indicates net-consumption of NPDOC compared to the treatment control.

Figure 3. (A) Relative abundance of the initial bacterial communities (top) and assemblage after a 6 month microcosm incubation (bottom) for each corresponding well from the PRB Birney field test site. (B) Canonical correspondence analysis (CCA) of the bacterial communities initially (purple) and the community after 6 month incubation (red) based on the bacterial OTU distribution by well with the replicates represented in parentheses next to the sample name. (C) Relative abundance of the initial archaeal community (top) and assemblage after a 6 month microcosm incubation (bottom) for each corresponding well from the PRB Birney field test site. (D) CCA of the initial archaeal community (purple) and the community after 6 month incubation (red) based on the archaeal OTU distribution by well with the replicates represented in parentheses next to the sample name.

Figure 4. Net changes in fluorescence after 6 months of incubation for representative excitation emission matrix spectra from low sulfate microcosms (FG and T), and high sulfate microcosms (K-09 and N-11).

Figure 5. (A) Excitation-Emission spectra of individual PARAFAC components C_1, C_2, C_3, and C_4 and (B) changes of fluorescence intensities of the same PARAFAC components over time for each of the sampled coal seam methane wells and their corresponding abiotic controls.

Figure 6. Canonical correspondence analysis (CCA) of the influence of identified PARAFAC components C_1, C_2, C_3, and C_4 (red vectors) on the relative abundance of (A) bacterial OTU profiles (97% sequence similarity) and (B) archaeal OTU profiles from sampled coal seam methane enrichments. Circles represent individual microcosm samples at the end of incubation.

References

Amend, J.P., Teske, A., 2005. Expanding frontiers in deep subsurface microbiology. Palaeogeogr. Palaeoclimatol. Palaeoecol. 219, 131–155. https://doi.org/10.1016/j.palaeo.2004.10.018

Baker, G.C., Smith, J.J., Cowan, D.A., 2003. Review and re-analysis of domain-specific 16S primers. J. Microbiol. Methods 55, 541–555. https://doi.org/10.1016/j.mimet.2003.08.009

Barnhart, E.P., Davis, K., Varonka, M.S., Orem, W.H., Cunningham, A.B., Ramsay, B.D., Fields, M.W., 2017. Enhanced coal-dependent methanogenesis coupled with algal biofuels: Potential water recycle and carbon capture. Int. J. Coal Geol. 171, 69–75.

876 Barnhart, E.P., De León, K.B., Ramsay, B.D., Cunningham, A.B., Fields, M.W., 2013.
877 Investigation of coal-associated bacterial and archaeal populations from a diffusive
878 microbial sampler (DMS). Int. J. Coal Geol. 115, 64–70.
879 https://doi.org/10.1016/j.coal.2013.03.006
880 Barnhart, E.P., Weeks, E.P., Jones, E.J.P., Ritter, D.J., McIntosh, J.C., Clark, A.C., Ruppert,
881 L.F., Cunningham, A.B., Vinson, D.S., Orem, W., Fields, M.W., 2016. Hydrogeochemistry
882 and coal-associated bacterial populations from a methanogenic coal seam. Int. J. Coal Geol.
883 162, 14–26. https://doi.org/10.1016/j.coal.2016.05.001
884 Beckmann, S., Luk, A.W.S., Gutierrez-Zamora, M.L., Chong, N.H.H., Thomas, T., Lee, M.,
885 Manefield, M., 2019. Long-term succession in a coal seam microbiome during in situ
886 biostimulation of coalbed-methane generation. ISME J. 13, 632–650.
887 https://doi.org/10.1038/s41396-018-0296-5
888 Borrel, G., Parisot, N., Harris, H.M.B., Peyretaillade, E., Gaci, N., Tottey, W., Bardot, O.,
889 Raymann, K., Gribaldo, S., Peyret, P., O'Toole, P.W., Bruge`re, J.F., 2014. Comparative
890 genomics highlights the unique biology of Methanomassiliicoccales, a Thermoplasmatales-
891 related seventh order of methanogenic archaea that encodes pyrrolysine. BMC Genomics
892 15, 679. https://doi.org/10.1186/1471-2164-15-679
893 Bouskill, N.J., Tang, J., Riley, W.J., Brodie, E.L., 2012. Trait-based representation of biological
894 nitrification: Model development, testing, and predicted community composition. Front.
895 Microbiol. 3, 364. https://doi.org/10.3389/fmicb.2012.00364
896 Bowman, J., 2006. The Methanotrophs — The Families Methylococcaceae and
897 Methylocystaceae, in: The Prokaryotes. pp. 266–289. https://doi.org/10.1007/0-387-30745-
898 1_15

899 Caporaso, J.G., Kuczynski, J., Stombaugh, J., Bittinger, K., Bushman, F.D., Costello, E.K.,
900 Fierer, N., Pẽa, A.G., Goodrich, J.K., Gordon, J.I., Huttley, G.A., Kelley, S.T., Knights, D.,
901 Koenig, J.E., Ley, R.E., Lozupone, C.A., McDonald, D., Muegge, B.D., Pirrung, M.,
902 Reeder, J., Sevinsky, J.R., Turnbaugh, P.J., Walters, W.A., Widmann, J., Yatsunenko, T.,
903 Zaneveld, J., Knight, R., 2010. QIIME allows analysis of high-throughput community
904 sequencing data. Nat. Methods 7, 335–336. https://doi.org/10.1038/nmeth.f.303
905 Carini, P., Marsden, P.J., Leff, J.W., Morgan, E.E., Strickland, M.S., Fierer, N., 2016. Relic
906 DNA is abundant in soil and obscures estimates of soil microbial diversity. Nat. Microbiol.
907 2, 16242. https://doi.org/10.1038/nmicrobiol.2016.242
908 Chen, M., Tong, H., Liu, C., Chen, D., Li, F., Qiao, J., 2016. A humic substance analogue AQDS
909 stimulates Geobacter sp. abundance and enhances pentachlorophenol transformation in a
910 paddy soil. Chemosphere 160, 141–148. https://doi.org/10.1016/j.chemosphere.2016.06.061
911 Cheng, L., Ding, C., Li, Q., He, Q., Dai, L. rong, Zhang, H., 2013. DNA-SIP Reveals That
912 Syntrophaceae Play an Important Role in Methanogenic Hexadecane Degradation. PLoS
913 One 8, 66784. https://doi.org/10.1371/journal.pone.0066784
914 Cheung, K., Sanei, H., Klassen, P., Mayer, B., Goodarzi, F., 2009. Produced fluids and shallow
915 groundwater in coalbed methane (CBM) producing regions of Alberta, Canada: Trace
916 element and rare earth element geochemistry. Int. J. Coal Geol. 77, 338–349.
917 https://doi.org/10.1016/j.coal.2008.07.012
918 Coble, P.G., 1996. Characterization of marine and terrestrial DOM in seawater using excitation-
919 emission matrix spectroscopy. Mar. Chem. 51, 325–346. https://doi.org/10.1016/0304-
920 4203(95)00062-3
921 Corseuil, H.X., Monier, A.L., Fernandes, M., Schneider, M.R., Nunes, C.C., Do Rosario, M.,

Alvarez, P.J.J., 2011. BTEX plume dynamics following an ethanol blend release: Geochemical footprint and thermodynamic constraints on natural attenuation. Environ. Sci. Technol. 45, 3422–3429. https://doi.org/10.1021/es104055q

Cory, R.M., Kaplan, L.A., 2012. Biological lability of streamwater fluorescent dissolved organic matter. Limnol. Oceanogr. 57, 1347. https://doi.org/10.4319/lo.2012.57.5.1347

Cory, R.M., McKnight, D.M., 2005. Fluorescence spectroscopy reveals ubiquitous presence of oxidized and reduced quinones in dissolved organic matter. Environ. Sci. Technol. 39, 8142–8149. https://doi.org/10.1021/es0506962

Cottrell, M.T., Kirchman, D.L., 2000. Community composition of marine bacterioplankton determined by 16S rRNA gene clone libraries and fluorescence in situ hybridization. Appl. Environ. Microbiol. 66, 5116–5122. https://doi.org/10.1128/AEM.66.12.5116-5122.2000

Cuetos, M.J., Gómez, X., Otero, M., Morán, A., 2010. Anaerobic digestion of solid slaughterhouse waste: Study of biological stabilization by Fourier Transform infrared spectroscopy and thermogravimetry combined with mass spectrometry. Biodegradation 21, 543–556. https://doi.org/10.1007/s10532-009-9322-7

D'Andrilli, J., Junker, J.R., Smith, H.J., Scholl, E.A., Foreman, C.M., 2019. DOM composition alters ecosystem function during microbial processing of isolated sources. Biogeochemistry 142, 281–298. https://doi.org/10.1007/s10533-018-00534-5

Dahm, K.G., Van Straaten, C.M., Munakata-Marr, J., Drewes, J.E., 2012. Identifying well contamination through the use of 3-D fluorescence spectroscopy to classify coalbed methane produced water. Environ. Sci. Technol. 47, 649–656. https://doi.org/10.1021/es303866k

Davey, K.E., Kirby, R.R., Turley, C.M., Weightman, A.J., Fry, J.C., 2001. Depth variation of

945 bacterial extracellular enzyme activity and population diversity in the northeastern North
946 Atlantic Ocean. Deep. Res. Part II Top. Stud. Oceanogr. 48, 1003–1017.
947 https://doi.org/10.1016/S0967-0645(00)00106-5
948 Davis, K.J., Lu, S., Barnhart, E.P., Parker, A.E., Fields, M.W., Gerlach, R., 2018. Type and
949 amount of organic amendments affect enhanced biogenic methane production from coal and
950 microbial community structure. Fuel 211, 600–608.
951 https://doi.org/10.1016/j.fuel.2017.09.074
952 Davis, K.J., Platt, G.A., Barnhart, E.P., Hiebert, R., Hyatt, R., Fields, M.W., Gerlach, R., 2019.
953 Biogenic coal-to-methane conversion can be enhanced with small additions of algal
954 amendment in field-relevant upflow column reactors. Fuel 256.
955 https://doi.org/10.1016/j.fuel.2019.115905
956 Ferrari, B.C., Binnerup, S.J., Gillings, M., 2005. Microcolony cultivation on a soil substrate
957 membrane system selects for previously uncultured soil bacteria. Appl. Environ. Microbiol.
958 71, 8714–8720. https://doi.org/10.1128/AEM.71.12.8714-8720.2005
959 Formolo, M., Martini, A., Petsch, S., 2008. Biodegradation of sedimentary organic matter
960 associated with coalbed methane in the Powder River and San Juan Basins, U.S.A. Int. J.
961 Coal Geol. 76, 86–97. https://doi.org/10.1016/j.coal.2008.03.005
962 Green, M.S., Flanegan, K.C., Gilcrease, P.C., 2008. Characterization of a methanogenic
963 consortium enriched from a coalbed methane well in the Powder River Basin, U.S.A. Int. J.
964 Coal Geol. 76, 34–45. https://doi.org/10.1016/j.coal.2008.05.001
965 Greub, G., Raoult, D., 2002. Parachlamydiaceae: Potential emerging pathogens. Emerg. Infect.
966 Dis. 8, 625–630. https://doi.org/10.3201/eid0806.010210
967 Haas, B.J., Gevers, D., Earl, A.M., Feldgarden, M., Ward, D. V., Giannoukos, G., Ciulla, D.,

968 Tabbaa, D., Highlander, S.K., Sodergren, E., Methé, B., DeSantis, T.Z., Petrosino, J.F.,
969 Knight, R., Birren, B.W., 2011. Chimeric 16S rRNA sequence formation and detection in
970 Sanger and 454-pyrosequenced PCR amplicons. Genome Res. 21, 434–504.
971 https://doi.org/10.1101/gr.112730.110
972 Hahn, M.W., Stadler, P., Wu, Q.L., Pöckl, M., 2004. The filtration-acclimatization method for
973 isolation of an important fraction of the not readily cultivable bacteria. J. Microbiol.
974 Methods 57, 379–390. https://doi.org/10.1016/j.mimet.2004.02.004
975 Hazen, R.M., Hemley, R.J., Mangum, A.J., 2012. Carbon in Earth's interior: Storage, cycling,
976 and life. Eos (Washington. DC). 93, 17–18. https://doi.org/10.1029/2012EO020001
977 Hoehler, T.M., Jørgensen, B.B., 2013. Microbial life under extreme energy limitation. Nat. Rev.
978 Microbiol. 11, 83–94. https://doi.org/10.1038/nrmicro2939
979 Huang, Z., Sednek, C., Urynowicz, M.A., Guo, H., Wang, Q., Fallgren, P., Jin, S., Jin, Y., Igwe,
980 U., Li, S., 2017. Low carbon renewable natural gas production from coalbeds and
981 implications for carbon capture and storage. Nat. Commun. 8.
982 https://doi.org/10.1038/s41467-017-00611-7
983 Huang, Z., Urynowicz, M.A., Colberg, P.J.S., 2013. Stimulation of biogenic methane generation
984 in coal samples following chemical treatment with potassium permanganate. Fuel 111, 813–
985 819. https://doi.org/10.1016/j.fuel.2013.03.079
986 Imachi, H., Sekiguchi, Y., Kamagata, Y., Loy, A., Qiu, Y.L., Hugenholtz, P., Kimura, N.,
987 Wagner, M., Ohashi, A., Harada, H., 2006. Non-sulfate-reducing, syntrophic bacteria
988 affiliated with Desulfotomaculum cluster I are widely distributed in methanogenic
989 environments. Appl. Environ. Microbiol. 72, 2080–2091.
990 https://doi.org/10.1128/AEM.72.3.2080-2091.2006

991 in ’t Zandt, M.H., Beckmann, S., Rijkers, R., Jetten, M.S.M., Manefield, M., Welte, C.U., 2018.
992 Nutrient and acetate amendment leads to acetoclastic methane production and microbial
993 community change in a non-producing Australian coal well. Microb. Biotechnol. 11.
994 https://doi.org/10.1111/1751-7915.12853
995 Jetten, M.S.M., Stams, A.J.M., Zehnder, A.J.B., 1992. Methanogenesis from acetate: a
996 comparison of the acetate metabolism in Methanothrix soehngenii and Methanosarcina spp.
997 FEMS Microbiol. Lett. 88, 181–197. https://doi.org/10.1016/0378-1097(92)90802-U
998 Kalyuzhnaya, M.G., Yang, S., Rozova, O.N., Smalley, N.E., Clubb, J., Lamb, A., Gowda,
999 G.A.N., Raftery, D., Fu, Y., Bringel, F., Vuilleumier, S., Beck, D.A.C., Trotsenko, Y.A.,
1000 Khmelenina, V.N., Lidstrom, M.E., 2013. Highly efficient methane biocatalysis revealed in
1001 a methanotrophic bacterium. Nat. Commun. 4, 2785. https://doi.org/10.1038/ncomms3785
1002 Kidnay, A.J., Parrish, W.R., 2006. Fundamentals of natural gas processing mechanical
1003 engineering., CRC Press. https://doi.org/10.1201/9781420014044
1004 Kulikova, N.A., Perminova, I. V., Badun, G.A., Chernysheva, M.G., Koroleva, O. V.,
1005 Tsvetkova, E.A., 2010. Estimation of uptake of humic substances from different sources by
1006 Escherichia coli cells under optimum and salt stress conditions by use of tritium-labeled
1007 humic materials. Appl. Environ. Microbiol. 76, 6223–6230.
1008 https://doi.org/10.1128/AEM.00905-10
1009 Lawaetz, A.J., Stedmon, C.A., 2009. Fluorescence intensity calibration using the Raman scatter
1010 peak of water. Appl. Spectrosc. 63, 936–940. https://doi.org/10.1366/000370209788964548
1011 Lepš, J., Šmilauer, P., 2006. Multivariate Analysis of Ecological Data, Bulletin of the Ecological
1012 Society of America. Cambridge University Press. https://doi.org/10.1890/0012-
1013 9623(2006)87[193:MAOED]2.0.CO;2

Lester, Y., Ferrer, I., Thurman, E.M., Sitterley, K.A., Korak, J.A., Aiken, G., Linden, K.G., 2015. Characterization of hydraulic fracturing flowback water in Colorado: Implications for water treatment. Sci. Total Environ. 512, 637–644. https://doi.org/10.1016/j.scitotenv.2015.01.043

Li, X., Dai, X., Takahashi, J., Li, N., Jin, J., Dai, L., Dong, B., 2014. New insight into chemical changes of dissolved organic matter during anaerobic digestion of dewatered sewage sludge using EEM-PARAFAC and two-dimensional FTIR correlation spectroscopy. Bioresour. Technol. 159, 412–420. https://doi.org/10.1016/j.biortech.2014.02.085

Liesack, W., Bak, F., Kreft, J.U., Stackebrandt, E., 1994. Holophaga foetida gen. nov., sp. nov., a new, homoacetogenic bacterium degrading methoxylated aromatic compounds. Arch. Microbiol. 162, 85–90. https://doi.org/10.1007/BF00264378

Liu, F., Guo, H., Wang, Q., Haider, R., Urynowicz, M.A., Fallgren, P.H., Jin, S., Tang, M., Chen, B., Huang, Z., 2019. Characterization of organic compounds from hydrogen peroxide-treated subbituminous coal and their composition changes during microbial methanogenesis. Fuel 237, 1209–1216. https://doi.org/10.1016/J.FUEL.2018.10.043

Logue, J.B., Stedmon, C.A., Kellerman, A.M., Nielsen, N.J., Andersson, A.F., Laudon, H., Lindström, E.S., Kritzberg, E.S., 2016. Experimental insights into the importance of aquatic bacterial community composition to the degradation of dissolved organic matter. ISME J. 10, 533–545. https://doi.org/10.1038/ismej.2015.131

Mao, C., Zhang, T., Wang, X., Feng, Y., Ren, G., Yang, G., 2017. Process performance and methane production optimizing of anaerobic co-digestion of swine manure and corn straw. Sci. Rep. 7, 9379. https://doi.org/10.1038/s41598-017-09977-6

Mara, D., Horan, N., 2003. Handbook of Water and Wastewater Microbiology, Academic Press.

https://doi.org/10.1016/B978-0-12-470100-7.X5000-6

McKnight, D.M., Boyer, E.W., Westerhoff, P.K., Doran, P.T., Kulbe, T., Andersen, D.T., 2001. Spectrofluorometric characterization of dissolved organic matter for indication of precursor organic material and aromaticity. Limnol. Oceanogr. 46, 38–48. https://doi.org/10.4319/lo.2001.46.1.0038

Miller, M.P., Simone, B.E., McKnight, D.M., Cory, R.M., Williams, M.W., Boyer, E.W., 2010. New light on a dark subject: Comment. Aquat. Sci. 72, 269–275. https://doi.org/10.1007/s00027-010-0130-2

Moore, T.A., 2012. Coalbed methane: A review. Int. J. Coal Geol. 101, 36–81. https://doi.org/10.1016/j.coal.2012.05.011

Murphy, K.R., Stedmon, C.A., Graeber, D., Bro, R., 2013. Fluorescence spectroscopy and multi-way techniques. PARAFAC. Anal. Methods 5, 6557–6566. https://doi.org/10.1039/c3ay41160e

Muyzer, G., Stams, A.J., 2008. The ecology and biotechnology of sulphate-reducing bacteria. Nat. Rev. 6, 441–454. https://doi.org/10.1038/nrmicro1892

Nobu, M.K., Narihiro, T., Rinke, C., Kamagata, Y., Tringe, S.G., Woyke, T., Liu, W.T., 2015. Microbial dark matter ecogenomics reveals complex synergistic networks in a methanogenic bioreactor. ISME J. 9, 1710–1722. https://doi.org/10.1038/ismej.2014.256

Orem, W.H., Tatu, C.A., Lerch, H.E., Rice, C.A., Bartos, T.T., Bates, A.L., Tewalt, S., Corum, M.D., 2007. Organic compounds in produced waters from coalbed natural gas wells in the Powder River Basin, Wyoming, USA. Appl. Geochemistry 22, 2240–2256. https://doi.org/10.1016/j.apgeochem.2007.04.010

Orem, W.H., Voytek, M.A., Jones, E.J., Lerch, H.E., Bates, A.L., Corum, M.D., Warwick, P.D.,

Clark, A.C., 2010. Organic intermediates in the anaerobic biodegradation of coal to methane under laboratory conditions. Org. Geochem. 41, 997–1000. https://doi.org/10.1016/j.orggeochem.2010.03.005

Pfeiffer, R., Ulrich, G., 2010. Chemical amendments for the stimulation of biogenic gas generation in deposits of carbonaceous material. US Pat. App. 12/751,745. https://doi.org/10.1023/A:1015575214292

Plugge, C.M., Zhang, W., Scholten, J.C.M., Stams, A.J.M., 2011. Metabolic flexibility of sulfate-reducing bacteria. Front. Microbiol. 2. https://doi.org/10.3389/fmicb.2011.00081

Pope, J., Herries, J., 2014. In-situ Detection and Analysis of Methane in Coal seam Methane Formations with Spectrometers. United States Pat. Appl. Publ.

Qiu, Y.L., Hanada, S., Ohashi, A., Harada, H., Kamagata, Y., Sekiguchi, Y., 2008. Syntrophorhabdus aromaticivorans gen. nov., sp. nov., the first cultured anaerobe capable of degrading phenol to acetate in obligate syntrophic associations with a hydrogenotrophic methanogen. Appl. Environ. Microbiol. 74, 2051–2058. https://doi.org/10.1128/AEM.02378-07

Qiu, Y.L., Sekiguchi, Y., Imachi, H., Kamagata, Y., Tseng, I.C., Cheng, S.S., Ohashi, A., Harada, H., 2004. Identification and Isolation of Anaerobic, Syntrophic Phthalate Isomer-Degrading Microbes from Methanogenic Sludges Treating Wastewater from Terephthalate Manufacturing. Appl. Environ. Microbiol. 70, 1617–1626. https://doi.org/10.1128/AEM.70.3.1617-1626.2004

Quast, C., Pruesse, E., Yilmaz, P., Gerken, J., Schweer, T., Yarza, P., Peplies, J., Glöckner, F.O., 2013. The SILVA ribosomal RNA gene database project: Improved data processing and web-based tools. Nucleic Acids Res. 41, 590–596. https://doi.org/10.1093/nar/gks1219

Rakoczy, J., Schleinitz, K.M., Müller, N., Richnow, H.H., Vogt, C., 2011. Effects of hydrogen and acetate on benzene mineralisation under sulphate-reducing conditions. FEMS Microbiol. Ecol. 77, 238–247. https://doi.org/10.1111/j.1574-6941.2011.01101.x

Reinhard, M., Hopkins, G.D., Steinle-Darling, E., LeBron, C.A., 2005. In situ biotransformation of BTEX compounds under methanogenic conditions. Gr. Water Monit. Remediat. 25, 50–59. https://doi.org/10.1111/j.1745-6592.2005.00046.x

Riley, S.M., Ahoor, D.C., Regnery, J., Cath, T.Y., 2018. Tracking oil and gas wastewater-derived organic matter in a hybrid biofilter membrane treatment system: A multi-analytical approach. Sci. Total Environ. 613, 208–217. https://doi.org/10.1016/j.scitotenv.2017.09.031

Ritter, Daniel, Vinson, D., Barnhart, E., Akob, D.M., Fields, M.W., Cunningham, A.B., Orem, W., McIntosh, J.C., 2015. Enhanced microbial coalbed methane generation: A review of research, commercial activity, and remaining challenges. Int. J. Coal Geol. 146, 28–41. https://doi.org/10.1016/j.coal.2015.04.013

Ritter, D., Vinson, D., Barnhart, E., Akob, D.M., Fields, M.W., Cunningham, A.B., Orem, W., McIntosh, J.C., 2015. Enhanced microbial coalbed methane generation: A review of research, commercial activity, and remaining challenges. Int. J. Coal Geol. 146, 28–41. https://doi.org/10.1016/j.coal.2015.04.013

Schink, B., 2005. Syntrophic Associations in Methanogenic Degradation. Mol. Basis Symbiosis 1–19.

Schink, B., 1997. Energetics of syntrophic cooperation in methanogenic degradation. Microbiol. Mol. Biol. Rev. 61, 262–280. https://doi.org/1092-2172/97/$04.0010

Schweitzer, H., Ritter, D., McIntosh, J., Barnhart, E., Cunningham, A.B., Vinson, D., Orem, W., Fields, M.W., 2019. Changes in microbial communities and associated water and gas

geochemistry across a sulfate gradient in coal seams: Powder River Basin, USA. Geochim. Cosmochim. Acta 245. https://doi.org/10.1016/j.gca.2018.11.009

Segata, N., Izard, J., Waldron, L., Gevers, D., Miropolsky, L., Garrett, W.S., Huttenhower, C., 2011. Metagenomic biomarker discovery and explanation. Genome Biol. 12, R60. https://doi.org/10.1186/gb-2011-12-6-r60

Sekhohola, L.M., Igbinigie, E.E., Cowan, A.K., 2013. Biological degradation and solubilisation of coal. Biodegradation 24, 305–318. https://doi.org/10.1007/s10532-012-9594-1

Siddique, T., Penner, T., Klassen, J., Nesbø, C., Foght, J.M., 2012. Microbial communities involved in methane production from hydrocarbons in oil sands tailings. Environ. Sci. Technol. 46, 9802–9810. https://doi.org/10.1021/es302202c

Stasik, S., Wick, L.Y., Wendt-Potthoff, K., 2015. Anaerobic BTEX degradation in oil sands tailings ponds: Impact of labile organic carbon and sulfate-reducing bacteria. Chemosphere 138, 133–139. https://doi.org/10.1016/j.chemosphere.2015.05.068

Stedmon, C.A., Bro, R., 2008. Characterizing dissolved organic matter fluorescence with parallel factor analysis: A tutorial. Limnol. Oceanogr. Methods 6, 572–579. https://doi.org/10.4319/lom.2008.6.572

Strapoć, D., Mastalerz, M., Dawson, K., MacAlady, J., Callaghan, A. V., Wawrik, B., Turich, C., Ashby, M., 2011. Biogeochemistry of microbial coal-bed methane. Annu. Rev. Earth Planet. Sci. 39. https://doi.org/10.1146/annurev-earth-040610-133343

Strong, P.J., Xie, S., Clarke, W.P., 2015. Methane as a resource: Can the methanotrophs add value? Environ. Sci. Technol. 49, 4001–4018. https://doi.org/10.1021/es504242n

Swinnen, I.A.M., Bernaerts, K., Dens, E.J.J., Geeraerd, A.H., Van Impe, J.F., 2004. Predictive modelling of the microbial lag phase: A review. Int. J. Food Microbiol. 94, 137–159.

https://doi.org/10.1016/j.ijfoodmicro.2004.01.006

Takahashi, S., Tomita, J., Nishioka, K., Hisada, T., Nishijima, M., 2014. Development of a prokaryotic universal primer for simultaneous analysis of Bacteria and Archaea using next-generation sequencing. PLoS One 9, 105592. https://doi.org/10.1371/journal.pone.0105592

Taylor, M., Ross, K., Bentham, R., 2009. Legionella, protozoa, and biofilms: Interactions within complex microbial systems. Microb. Ecol. https://doi.org/10.1007/s00248-009-9514-z

Teeling, H., Fuchs, B.M., Becher, D., Klockow, C., Gardebrecht, A., Bennke, C.M., Kassabgy, M., Huang, S., Mann, A.J., Waldmann, J., Weber, M., Klindworth, A., Otto, A., Lange, J., Bernhardt, J., Reinsch, C., Hecker, M., Peplies, J., Bockelmann, F.D., Callies, U., Gerdts, G., Wichels, A., Wiltshire, K.H., Glöckner, F.O., Schweder, T., Amann, R., 2012. Substrate-controlled succession of marine bacterioplankton populations induced by a phytoplankton bloom. Science (80-.). 336, 608–611. https://doi.org/10.1126/science.1218344

Tomei, M.C., Rita, S., Mininni, G., 2011. Performance of sequential anaerobic/aerobic digestion applied to municipal sewage sludge. J. Environ. Manage. 92, 1867–1873. https://doi.org/10.1016/j.jenvman.2011.03.016

Ulrich, G., Bower, S., 2008. Active methanogenesis and acetate utilization in Powder River Basin coals, United States. Int. J. Coal Geol. 76, 25–33. https://doi.org/10.1016/j.coal.2008.03.006

Valero, N., Gómez, L., Pantoja, M., Ramírez, R., 2014. Production of humic substances through coal-solubilizing bacteria. Brazilian J. Microbiol. 45, 911–918. https://doi.org/10.1590/S1517-83822014000300021

Van Voast, W.A., 2003. Geochemical signature of formation waters associated with coalbed

methane. Am. Assoc. Pet. Geol. Bull. 87, 667–676. https://doi.org/10.1306/10300201079

Vick, S.H.W., Greenfield, P., Tran-Dinh, N., Tetu, S.G., Midgley, D.J., Paulsen, I.T., 2018. The Coal Seam Microbiome (CSMB) reference set, a lingua franca for the microbial coal-to-methane community. Int. J. Coal Geol. 186, 41–50. https://doi.org/10.1016/J.COAL.2017.12.003

Vinson, D.S., Blair, N.E., Martini, A.M., Larter, S., Orem, W.H., McIntosh, J.C., 2017. Microbial methane from in situ biodegradation of coal and shale: A review and reevaluation of hydrogen and carbon isotope signatures. Chem. Geol. 453, 128–145. https://doi.org/10.1016/j.chemgeo.2017.01.027

Wang, Q., Garrity, G.M., Tiedje, J.M., Cole, J.R., 2007. Naïve Bayesian classifier for rapid assignment of rRNA sequences into the new bacterial taxonomy. Appl. Environ. Microbiol. 73, 5264–5267. https://doi.org/10.1128/AEM.00062-07

Watve, M., Shejval, V., Sonawane, C., Rahalkar, M., Matapurkar, A., Shouche, Y., Patole, M., Phadnis, N., Champhenkar, A., Damle, K., Karandikar, S., Kshirsagar, V., Jog, M., 2000. The “K” selected oligophilic bacteria: A key to uncultured diversity? Curr. Sci. 78, 1535–1542. https://doi.org/10.1177/0022487110369555

Wawrik, B., Mendivelso, M., Parisi, V.A., Suflita, J.M., Davidova, I.A., Marks, C.R., Van Nostrand, J.D., Liang, Y., Zhou, J., Huizinga, B.J., Strapoć, D., Callaghan, A. V., 2012. Field and laboratory studies on the bioconversion of coal to methane in the San Juan Basin. FEMS Microbiol. Ecol. 81, 26–42. https://doi.org/10.1111/j.1574-6941.2011.01272.x

Yamamoto, K., Tamaki, H., Cadillo-Quiroz, H., Imachi, H., Kyrpides, N., Woyke, T., Goodwin, L., Zinder, S.H., Kamagata, Y., Liu, W.-T., 2014. Complete Genome Sequence of Methanoregula formicica SMSPT, a Mesophilic Hydrogenotrophic Methanogen Isolated

from a Methanogenic Upflow Anaerobic Sludge Blanket Reactor. Genome Announc. 2, e00870-14. https://doi.org/10.1128/genomeA.00870-14

Yu, Z., Chistoserdova, L., 2017. Communal metabolism of methane and the rare earth element switch. J. Bacteriol. 199, 328–345. https://doi.org/10.1128/JB.00328-17

Zengler, K., Richnow, H.H., Rosselló-Mora, R., Michaelis, W., Widdel, F., 1999. Methane formation from long-chain alkanes by anaerobic microorganisms. Nature 601, 266–269. https://doi.org/10.1038/45777

Zhao, Z., Zhang, Y., Ma, W., Sun, J., Sun, S., Quan, X., 2016. Enriching functional microbes with electrode to accelerate the decomposition of complex substrates during anaerobic digestion of municipal sludge. Biochem. Eng. J. 111, 1–9. https://doi.org/10.1016/j.bej.2016.03.002

Figures

Figure 1.

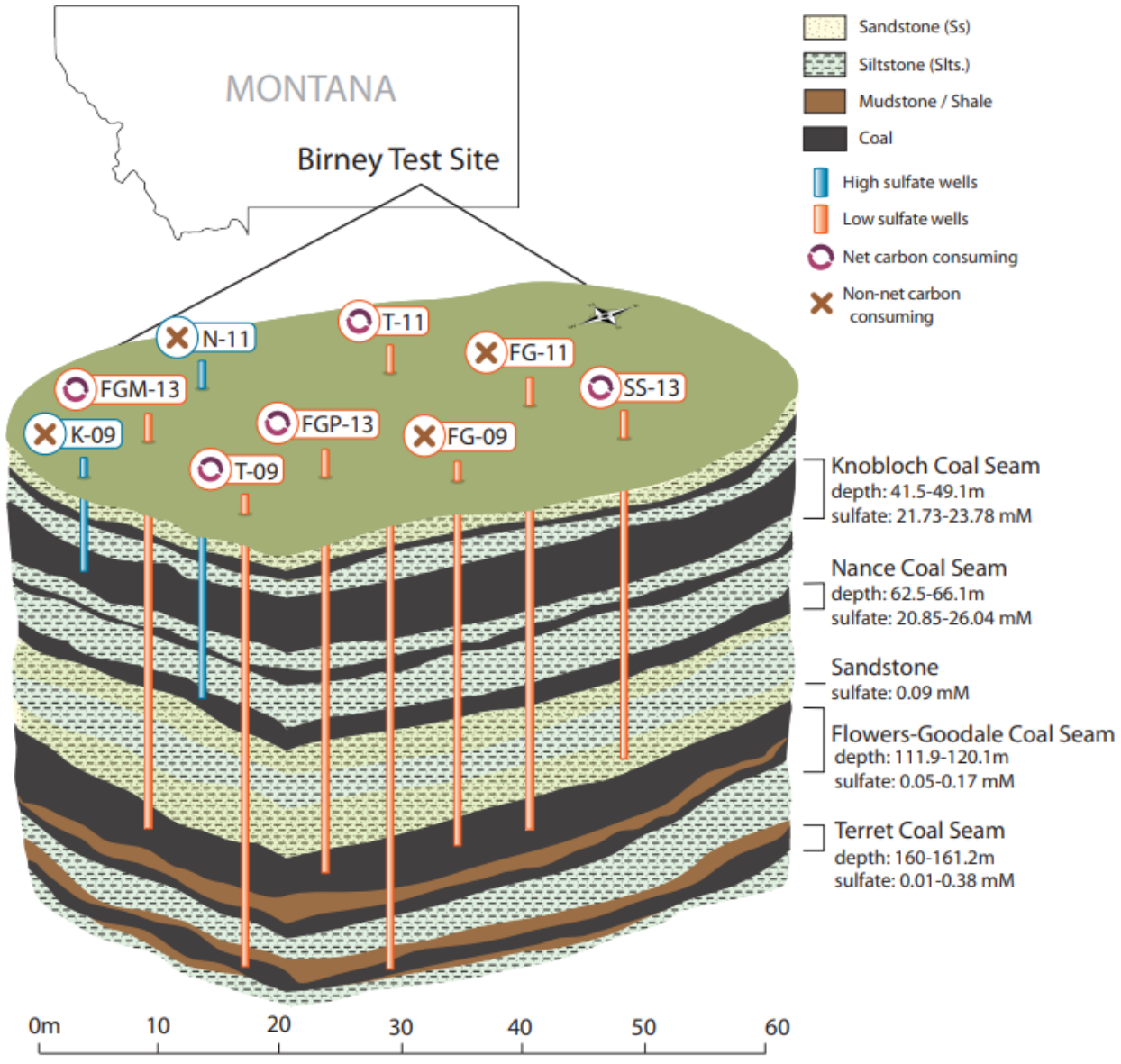

1206 Figure 2.

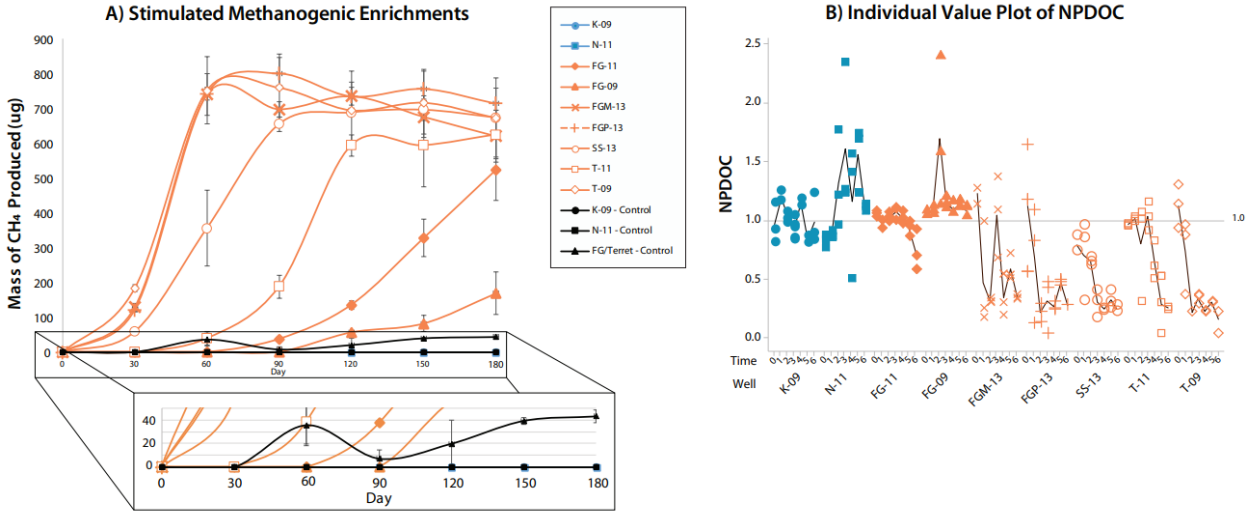

1207

1208 Figure 3.

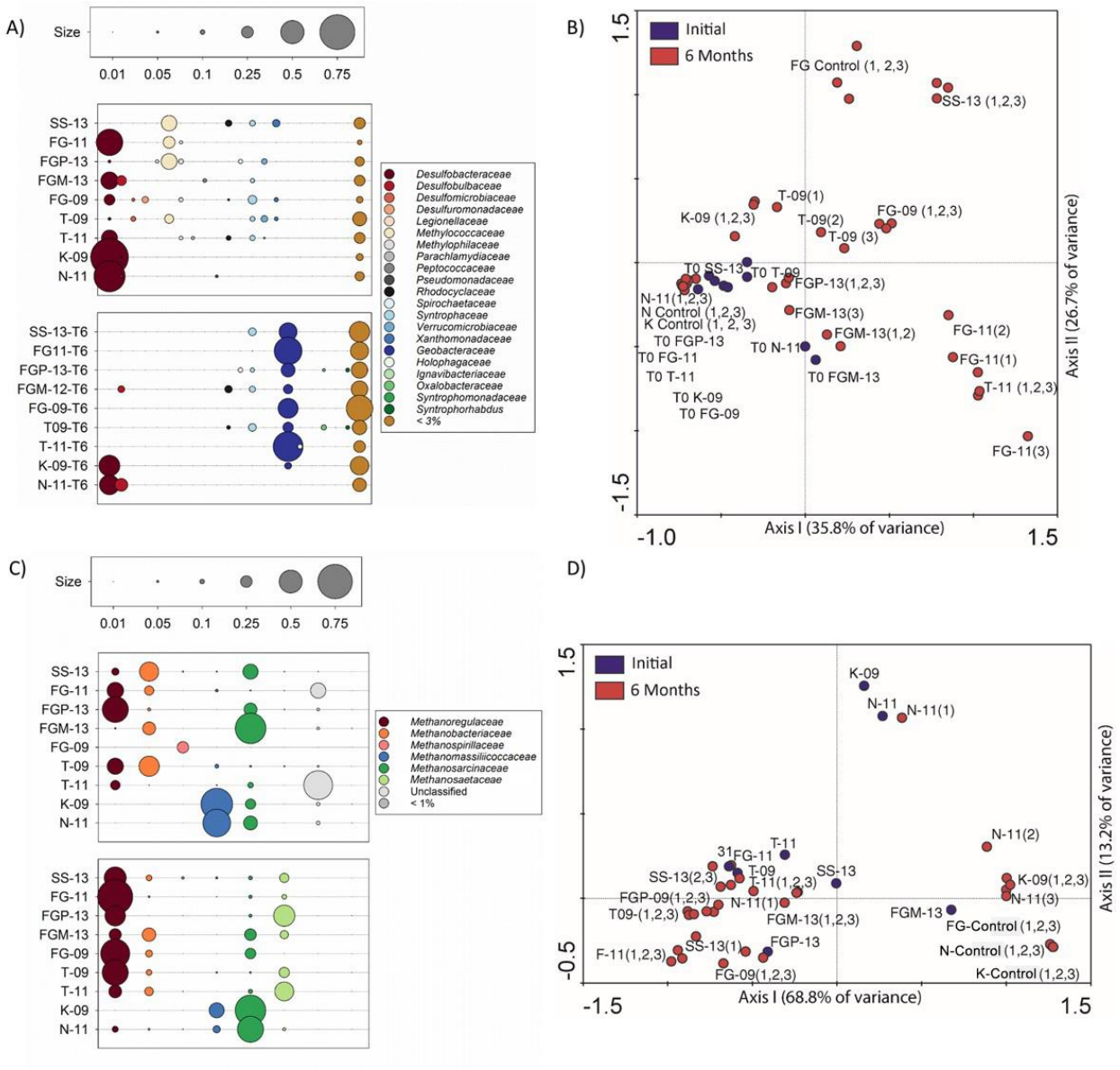

1209

1210

1211

1212

1213 Figure 4.

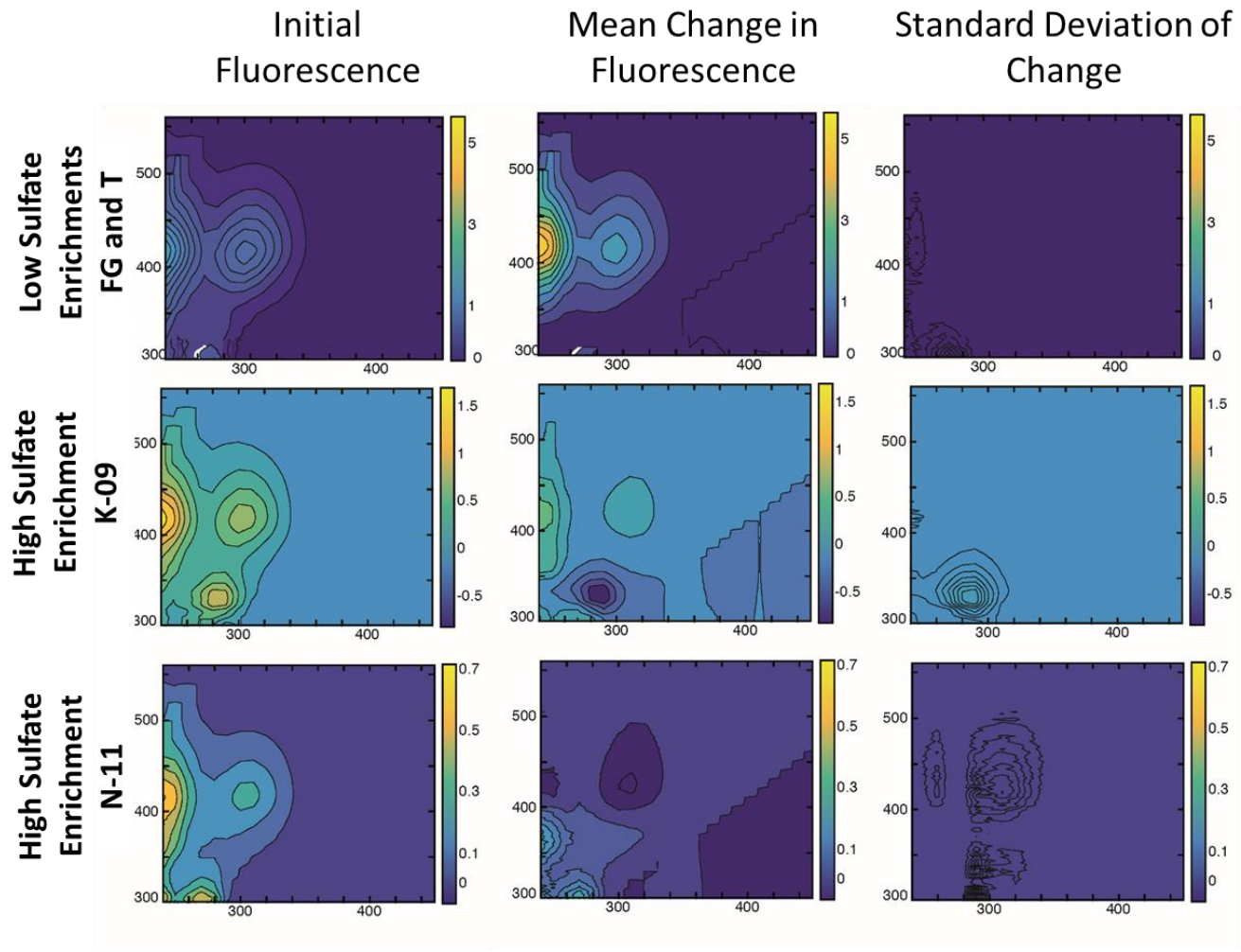

1214

1215

1216 Figure 5.

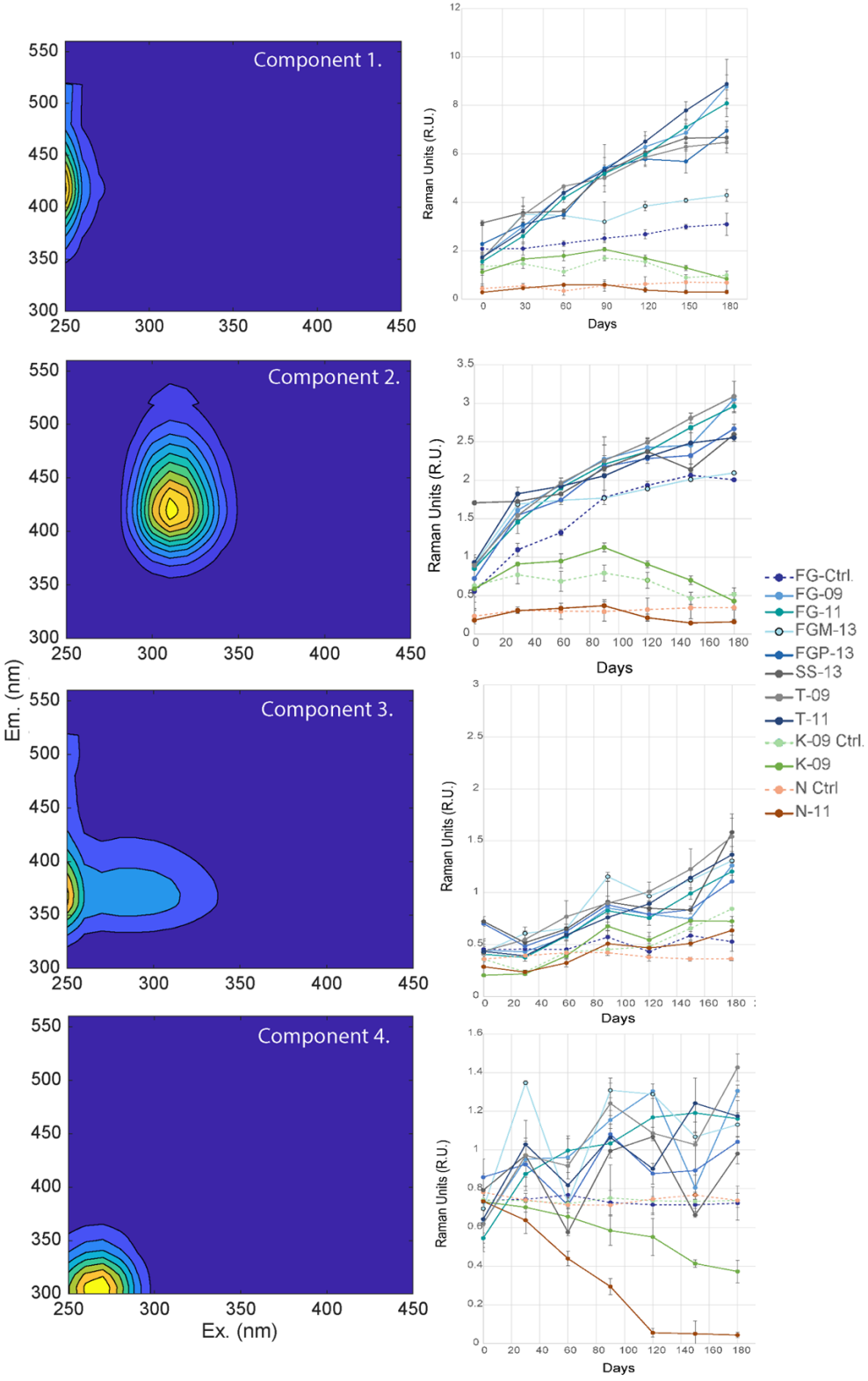

1217

1218

1219 Figure 6.

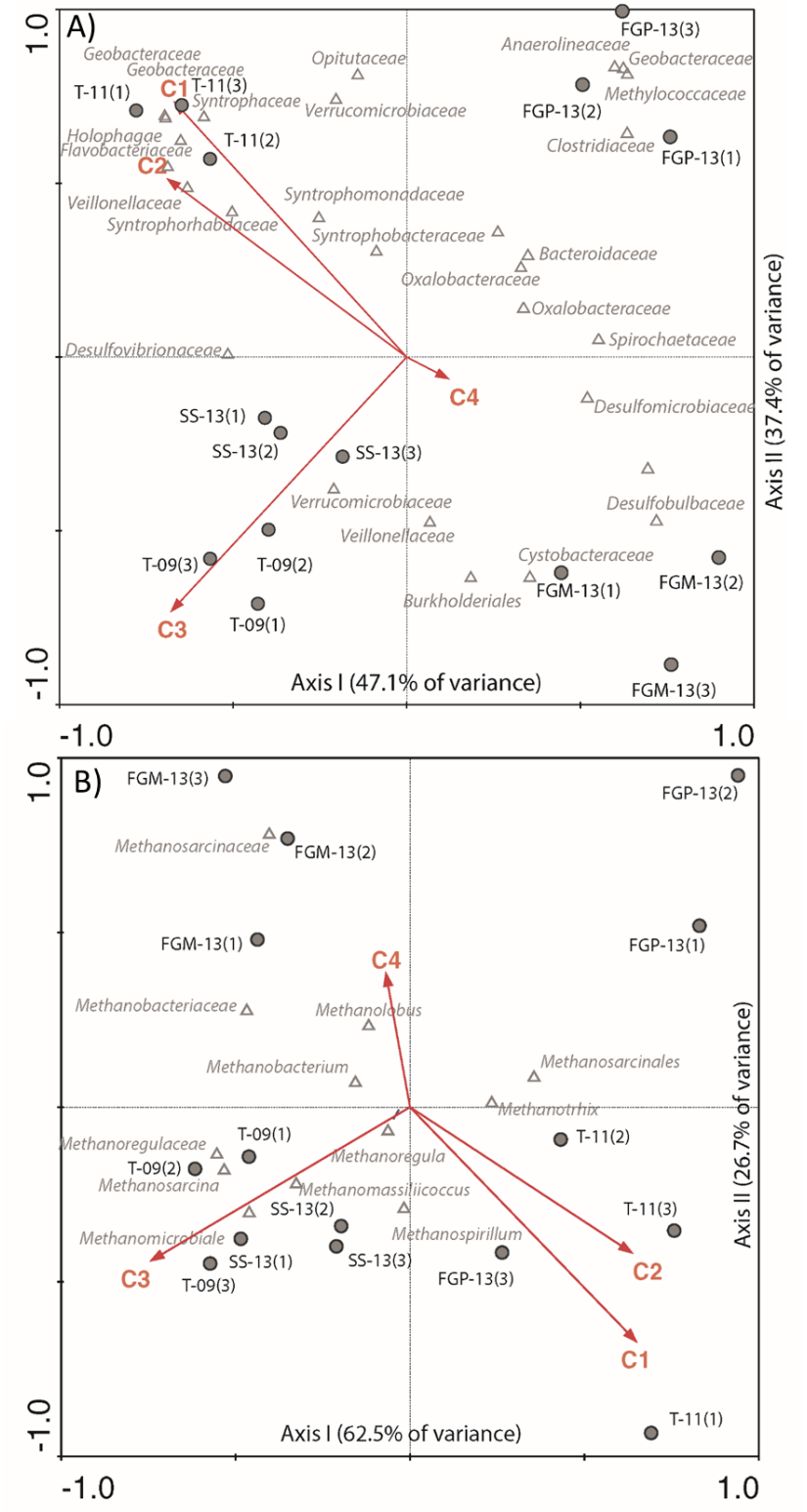

1220